Marine Geology 264 (2009) 74–97

Contents lists available at ScienceDirect

Marine Geology

journal homepage: www.elsevier.com/locate/margeo

A probabilistic approach for determining submarine landslide tsunami hazard along the upper east coast of the United States

Stephan T. Grilli *, Oliver-Denzil S. Taylor, Christopher D.P. Baxter, Stefan Maretzki

Departments of Ocean/Civil and Environmental Engineering, University of Rhode Island, Narragansett, RI, 02882, USA

ARTICLE INFO

Article history:
Received 7 February 2008
Received in revised form 14 January 2009
Accepted 25 February 2009

Keywords:
submarine mass movements
tsunami triggering
probabilistic analysis tsunami hazard
Monte Carlo modeling
runup analysis

ABSTRACT

Tsunami hazard assessment is critical for coastal communities, emergency services, and industry, to develop regional risk and response management plans, for catastrophic tsunami events (such as the recent 1998 Papua New Guinea (PNG) and 2004 Indian Ocean tsunamis). Along the northeastern United States coastline, tsunami hazard assessment is in its infancy, mostly due to the lack of historical tsunami record and the uncertainty regarding the return periods of potential large-scale events. The latter includes large transoceanic tsunamis, such as could be caused by a collapse of the Cumbre Vieja volcano in the Canary Islands or a large co-seismic tsunami initiated in the Puerto Rican trench, as well as large local tsunamis, such as could be caused by a Submarine Mass Failure (SMF) occurring on the nearby continental slope. In this region, considerable geologic and some historical (e.g., the 1929 Grand Bank landslide tsunami) evidence suggests that the largest tsunami hazard may arise from tsunamigenic SMFs, triggered by moderate seismic activity. The coastal impact of SMF (or landslide) tsunamis, indeed, can potentially be narrowly focused and affect specific communities.

This research presents the development, validation, and results of a probabilistic geomechanical and coastal tsunami impact analysis, of tsunami hazard on the upper northeast coast of the United States. Results are presented in terms of nearshore breaking wave height and runup, caused by seismically induced tsunamigenic SMF, with a given return period. A Monte Carlo approach is employed, in which distributions of relevant parameters (seismicity, sediment properties, type and location, volume, and dimensions of slide, water depth, etc.) are used to perform large numbers of stochastic stability analyses of submerged slopes (along actual shelf transects), based on standard pseudo-static limit equilibrium methods. The distribution of predicted slope failures along the upper U.S. East Coast is found to match published data quite well.

For slopes that are deemed unstable for a specified ground acceleration (with given return period), the tsunami source characteristic height is found using empirical equations (based on earlier numerical simulation work), and corresponding breaking height and runup are estimated on the nearest coastline. For a 0.2% annual-probability ground acceleration, for instance, simulations yield a return period of tsunamigenic SMFs of 3350-yr (i.e., a 0.03% annual probability of occurrence). The resulting estimate of the overall coastal hazard, from 100 and 500-yr SMF tsunami events, is found to be quite low at most locations, as compared to the typical 100 yr hurricane storm surge in the region (~4–5 m). Specifically, for the 100 yr event, SMF tsunami hazard is quite low with no coastal region exceeding a 1 m runup. For the 500 yr event, however, two regions of relatively elevated hazard are found: (1) near Long Island, NY, with a peak runup of 3 m; and (2) near the New Jersey coast, with a peak runup of 4 m. It should be stressed that these are only first-order estimates and detailed tsunami inundation modeling is required to fully quantify tsunami runup (and inundation) at these sites. This will be the object of more detailed studies in future work.

© 2009 Elsevier B.V. All rights reserved.

1. Introduction

Tsunamis can be generated by volcanic eruptions, co-seismic ocean bottom motion, subaerial and submarine mass movements (or failures, i.e., SMF), and oceanic meteorite impacts. The NGDC Tsunami Event Database (NOAA, 2008) documents approximately 2275 historical tsunami events worldwide, with varying failure mechanisms. Among these events, approximately 1600 (70%) tsunamis are considered to have resulted from seismic activity and 175 are attributed to SMFs of various sizes and mechanisms, with 73 of those triggered by earthquakes, including 61 positively confirmed and 12 either unconfirmed or questionable events. Within these 61 confirmed cases, 34 (56%) resulted from moderate earthquakes (M_w<7.0). [It must be noted that these statistics do not include submarine landsides, or tsunamis, of unknown triggering mechanism. Furthermore, considerable uncertainty exists within the

* Corresponding author. Tel.: +1 401 874 6636; fax: +1 401 874 6837.
E-mail address: grilli@oce.uri.edu (S.T. Grilli).

0025-3227/$ – see front matter © 2009 Elsevier B.V. All rights reserved.
doi:10.1016/j.margeo.2009.02.010

Historical Database due to many tsunami events prior to the 1950's being attributed to co-seismic triggers, when the true tsunami mechanism should have been a submarine failure. This is due mostly to the lack of knowledge, historically, concerning not only tsunami generation but the existence of tsunamigenic submarine failures. Therefore, only noticeable triggers (e.g. volcanic eruption, seismic activity, etc.) were considered as potential tsunami triggering mechanisms and recorded as such within the NGDC Database.]

To date, co-seismic bottom motion has been the most extensively studied and modeled tsunami generation mechanism, likely because it is responsible for the largest and most energetic recorded events. In the past decade, however, following the 1998 Papua New Guinea (PNG) landslide tsunami, which caused great damage and loss of life (2000 fatalities, e.g., Tappin et al., 2001, 2002, 2008), a large amount of physical and numerical modeling work has been devoted to studying SMF tsunami generation (e.g., Heinrich, 1992; Grilli and Watts, 1999; Watts et al., 2000; Grilli and Watts, 2001; Ward, 2001; Tinti et al., 2001; Grilli et al., 2002; Lynett and Liu, 2003; Enet et al., 2003; Watts et al., 2003; Watts and Grilli, 2003; Locat et al., 2004; Fine et al., 2005; Liu et al., 2005; Haugen et al., 2005; Watts et al., 2005a; Grilli and Watts, 2005; Enet and Grilli, 2005, 2007; see extensive literature reviews in some of these papers). In fact, it is being increasingly recognized, by both the research and tsunami forecasting communities, that earthquakes affecting oceanic margins can frequently trigger SMFs. Although many of these will not be tsunamigenic, a few could potentially generate significant near-field tsunamis, even if the earthquake magnitude is not sufficient to generate a significant co-seismic tsunami. In approximately 35% of all cases, nearshore waves from landslide tsunamis could even exceed those resulting solely from co-seismic ground motions (Watts, 2004). Finally, the majority of tsunamigenic SMFs occur for bottom slope angles less than 5° (Canals et al., 2004).

As our understanding of the potential risk associated with tsunamigenic SMFs increases, so does the importance of assessing their potential hazard to coastal communities. This is of particular importance for heavily populated coastal regions, such as the northeastern United States, that do not have high local co-seismic tsunami risks but could have elevated SMF tsunami risks. The understanding and quantification of such risks is essential, when considering typical return periods for large seismic events (e.g., 100 and 500 yr), because possible coastal inundation (and runup) levels from seismically induced SMF tsunamis could locally exceed inundation levels from other hazards with similar return period, such as hurricanes, and hence influence design and development considerations for major coastal structures and communities.

The need for tsunamigenic SMF hazard assessment in such areas can be best illustrated by the Papua New Guinea tsunami, which was generated by a rotational SMF (a.k.a. slump), triggered by a 7.2 magnitude earthquake. While only a moderate co-seismic tsunami runup was generated (~1 m), 15 min later, the slump occurred, creating a tsunami that caused up to 16 m runup on a nearby low-lying barrier island (Sissano Lagoon), and 2000 fatalities among people who were totally unaware that an earthquake had occurred (e.g., Tappin et al., 2001, 2002, 2008 and other papers listed in those references). Additionally, since submarine mass movements typically occur on or near the continental shelf break, tsunami warning times may range from only tens of minutes to a couple of hours at most, rather than typically several hours for large transoceanic co-seismic tsunamis. Such small warning times could potentially increase the human death toll (as in the case of the Papa New Guinea event).

An accurate tsunami hazard assessment for the U.S. Northeast is difficult, due in part to the lack (or great paucity) of direct tsunami observations within the historical records (NGDC Tsunami Event Database, NOAA, 2008) and the uncertainty regarding return periods of past large-scale events, whose impact in terms of paleo-sediment deposits has been identified in the literature (e.g., Goodbred et al., 2006). Hence, to develop a comprehensive tsunami hazard assessment for the U.S. Northeast, one first need to identify the various mechanisms and sources that could generate both local and transoceanic tsunamis affecting the coast.

There is only one significant co-seismic source in the Western North Atlantic, from a seism occurring in the 600 km long deep trench North of Puerto Rico (18° N Lat). There are no other major subduction zones in the upper North Atlantic Ocean, in which a potentially large earthquake could occur. The generation of an extreme co-seismic tsunami (e.g., magnitude 9) in the Puerto Rican trench was studied by Knight (2006) and Knight and Banks (personal communication), with focus on impacts for the Caribbean islands and the Gulf of Mexico; the impact of the same scenario on the U.S. East Coast was simulated by the lead author and co-workers (Pérignon, 2006). Although greatly affecting the Caribbean islands, it was found that such an event would only cause limited runup on the upper U.S. East Coast. The flank collapse of the Cumbre Vieja volcano in the Canary Islands was also proposed as a potential extreme transoceanic tsunami source in the North Atlantic Ocean (Elsworth and Day, 1999; Ward and Day, 2001; Hildenbrand et al., 2003), as well as a repeat of the Lisbon 1755 tsunami. Tsunami propagation for a more recently proposed extreme scenario of the Cumbre Vieja collapse (Day, personal communication, 2006) was also simulated by the lead author and co-workers and found to cause limited runup on the upper U.S. East Coast (Pérignon, 2006).

The work presented here, hence, concentrates on assessing additional tsunami hazard from local sources, for the U.S. Northeast, which primarily involves SMFs that could be triggered on the nearby continental slope, by local (or regional) earthquakes of moderate magnitude. The upper east coast of the United States has a wide continental shelf with considerable geologic evidence of submarine mass movements (e.g. Booth et al., 1985; Booth et al., 1993; Piper et al., 2003; Locat et al., 2003, Chaytor et al., 2007, 2009-this issue). The work by Booth et al. (1993), with later refinements by Chaytor et al. (2007, 2009-this issue), identified the characteristics of between 55 and 179 past individual SMFs on the northeast U.S. Atlantic outer continental margin.

The largest earthquake on record for the upper North Atlantic region is a 7.2 magnitude earthquake, which in 1929 triggered a large debris flow off of the Grand Banks, generating a tsunami that caused 27 fatalities and extensive damage in Newfoundland, with impacts extending to northern Maine (Piper et al., 1999; Trifunac et al., 2002; Fine et al., 2005). Earthquakes of lower magnitude (i.e., 6–7) could happen more frequently in the region and potentially trigger tsunamigenic SMFs, causing narrowly focused tsunamis (Ward, 2001; Grilli et al., 2002; Rabinovich et al., 2003; Enet and Grilli, 2007) with initial wave heights much greater than those solely generated by the vertical co-seismic bottom displacement. In addition to their directionality, the fact that SMF tsunamis can be triggered quite close to shore implies that resulting runup and inundation may potentially be very significant for localized coastal regions, despite their much lower total energy release than for large co-seismic events.

For large individual transoceanic events, once a tsunami source scenario has been identified and parameterized, based on seismological and/or geological hypotheses, direct simulations are usually performed with a long wave propagation model, for a number of scenarios affecting a specific region (typically up to a few dozen). Provided accurate ocean and coastal bottom bathymetry and topography are available, and a fine enough coastal grid is used in the model, reasonable estimates of runup distributions and inundation areas can be made, that can be used to create tsunami hazard maps. There are numerous examples of using this approach in the literature, for both potential future and past events (i.e., in a hindcast mode), such as the recent catastrophic December 26, 2004 Indian Ocean tsunami (e.g., Titov et al., 2005; Watts et al., 2005b; Grilli et al., 2007; Ioualalen et al., 2007). The same methodology was also applied to past SMF

tsunami case studies, to provide a better understanding of the events (e.g., Watts et al., 2003; Day et al., 2005; Tappin et al., 2008).

As indicated before, in this work, we aim at assessing tsunami risks for the U.S. Northeast coast, associated with local, potentially tsunamigenic SMFs. To quantify such risks in a probabilistic manner, however, it is impractical not only to attempt to concurrently consider all slope failure mechanisms (e.g., seismic activity, rapid sedimentation, increase in pore water pressures, gas hydrate dissipation, etc.), but also to perform direct numerical simulations for the large number of potential scenarios required for a proper risk assessment (due to uncertainties in landslide location, the many parameters affecting SMF tsunami generation, and uncertainties in physical values of these). Therefore, we focus on assessing coastal hazard only from the most common failure mechanism, seismic activity, and on estimating generated tsunami heights and runup, based on simple but experimentally validated empirical equations, derived from earlier numerical simulation work (Grilli and Watts, 2005; Watts et al., 2005a; Enet and Grilli, 2007). Therefore, in this work we present the development, validation, and results of a probabilistic model of seismically triggered SMF tsunamis and induced coastal hazard, for the Upper U.S. East Coast.

This objective is accomplished using a Monte Carlo Simulation (MCS) model (e.g., Harr, 1987; Watts, 2004), in which probability distribution functions of governing parameters (e.g., slide density, friction angle, etc.), treated as random variables, are used (when known) or estimated, and from these distributions the model randomly generates a large number of plausible combinations of parameter values. In the present case, properties of a section of continental slope (both geometrical and physical), along a series of specified transects, are generated for many MCS trials and, based on these, slope stability is calculated (using standard pseudo-static analyses), under specified seismic loading (i.e., horizontal acceleration). Provided enough simulations are performed, the resulting SMF probability (and return period) can be assumed to approximate actual conditions (i.e., the solution of a complex problem, for which no closed-form solution can otherwise be obtained). Nearshore tsunami hazard is then similarly quantified, using simplified tsunami generation, propagation, and runup calculation procedures, which yield statistics of runup distributions.

The following sections detail the MCS model development and validation, as well as its application to the U.S. northeast coast. Results are finally presented in terms of 100 and 500 yr design tsunami events, which offer a first-order regional scale SMF tsunami hazard assessment. The latter is used to identify regional areas of the U.S. northeastern coastline exhibiting potentially increased SMF tsunami hazard.

2. Monte Carlo model

2.1. Overview

The probabilistic analysis, which is at the core of our study of regional landslide (i.e., SMF) tsunami hazard along the upper U.S. East Coast, is performed using a newly developed Monte Carlo Simulation (MCS) model. In MCSs, stochastic analyses are performed, based on input data having a certain level of uncertainty. Thus, instead of specifying discrete values of governing parameters for a limited number of analyses (as is done in a deterministic analysis), a large number of MCS trials are performed, for randomly selected parameter values within their known (or estimated) probability distributions (e.g., uniform, normal, log-normal, etc…). MCS results are similarly expressed in terms of probability distributions, which can then be validated by comparison to known distributions for some of the outputs, and used to determine probabilities of occurrence of failure, runup, etc. By applying such a MCS methodology, we are able to quantify SMF tsunami hazard in terms of its probability of occurrence.

Specifically, in this work, distributions of governing parameters affecting SMFs (i.e., seismicity, sediment properties, type and location of failures, failure volume, water depth, etc…; see Table 1 for a full list) are specified in the MCS model on the basis of field observations (e.g., Booth et al., 1993). Using these, thousands of stochastic submarine slope stability analyses are performed along a series of transects (45) laid across the study area, from shallower to deeper water (Fig. 1a). Transects are carefully selected to best represent continental slope areas (or sections) having fairly homogeneous topographic features. Slope stability analyses are performed using the actual bathymetry along each of those transects (Fig. 1b), based on standard pseudo-static limit equilibrium methods, for either translational or rotational failures (see details below). [Indeed, our geologic study area displays evidence of both failure types, at least initially, as noted by Booth et al. (1993). Chaytor et al. (2007) identifies three landslide types; rotational, translational, and debris flows.] Accordingly, given a set of randomly selected physical parameters and a peak horizontal ground acceleration associated with a selected seismic return period, slope failure is deemed to occur when the factor of safety of the selected slope section is less than unity. For each recognized failure in the MCS trials, a characteristic tsunami height is calculated, together

Table 1
Random input parameters used in MCS simulations.

Parameter	Failure type	Distribution	Mean	Value	Remarks
Depth to failure d	Translational	Log-normal	1113	[mbsl]	The water depth to the upslope edge of failure is constrained to between 120 and 2500 m below sea level.
	Rotational	Log-normal	1241	[mbsl]	
SMF length l	Translational	Log-normal	4917	[m]	The SMF length l is constrained based on the actual slope bathymetry, as no failure is assumed to occur shallower than the slope crest, or deeper than its toe. Minimum and maximum translational length are (1000, 50,000) m. Minimum and maximum rotational length are (1000, 4000) m.
	Rotational	Log-normal	2063	[m]	
SMF thickness T	Translational	Log-normal	125	[m]	The SMF thickness is obtained from a uniformly distributed thickness-to-length ratio T/l within [0.01,0.04] (translational) and [0.07,0.20] (rotational). (Watts et al., 2005a)
	Rotational	Log-normal	256	[m]	
SMF bulk density ρ_s	Translational	Normal	1.840	[g/cm^3]	Based on the finding of ODP Leg 174A. ρ_s is a function of depth to failure plus the depth to the point of interest within the SMF thickness. The average ρ_s over the SMF thickness is assumed normally distributed in the MCS model. [Due to the limited sediment data, this is the parameter with the highest degree of uncertainty.]
	Rotational	Normal	1.815	[g/cm^3]	
SMF slope angle β	Translational	Log-normal	3.5	[degrees]	The SMF slope angle is calculated from the actual bathymetry along each transect, after randomly selecting the SMF depth and length. The SMF slope is found to follow a log-normal distribution. [This distribution does not include slope angles that do not produce failure.] Due to the randomly selected sediment type/properties and strength reduction factor, the mean slope angle required to initiate failure varies significantly for each failure type.
	Rotational	Log-normal	10.2	[degrees]	

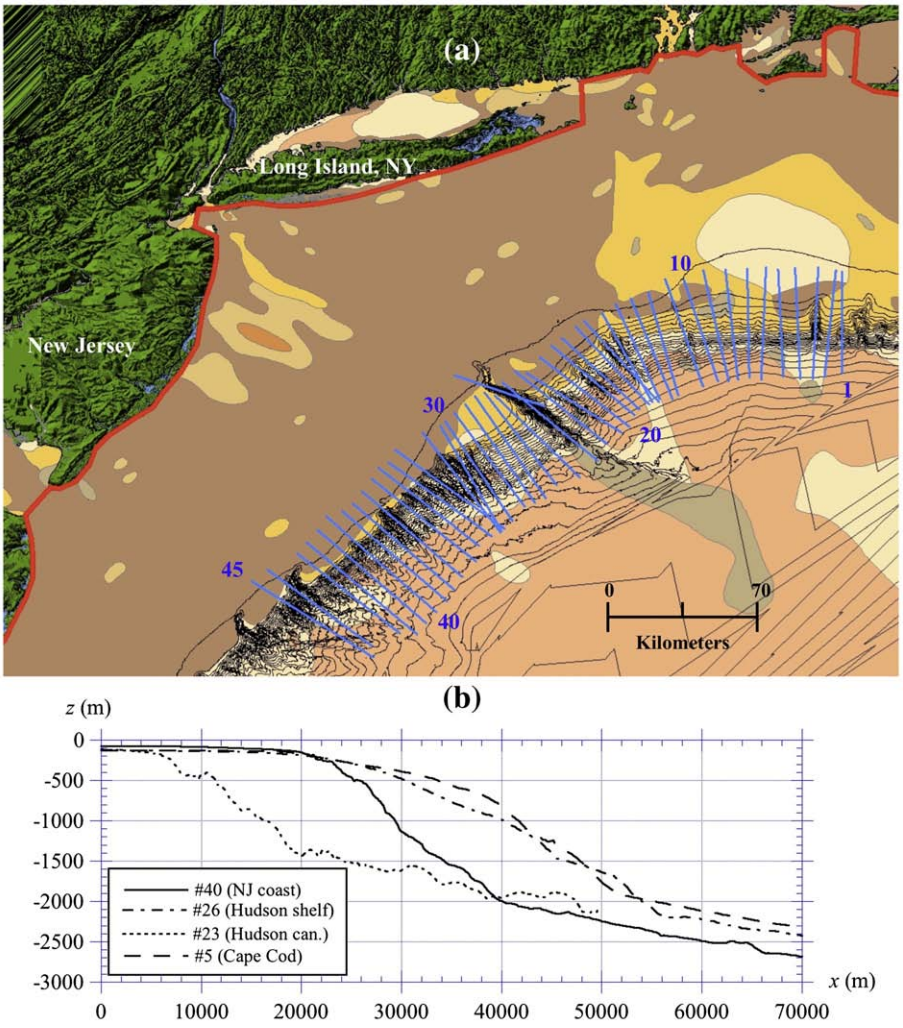

Fig. 1. (a) Idealized coastline (thick red line) in the study area, with transects (thick blue lines) utilized in the MCS model; (b) Bathymetry for 4 typical transects. (For interpretation of the references to colour in this figure legend, the reader is referred to the web version of this article.)

with the resulting runup (and breaking wave height) on nearby shores.

Watts (2004) first proposed to use a MCS approach to estimate landslide tsunami risk in Southern California. His MCS model, however, was entirely empirical and no stability analyses were performed. During the course of this work, an initial Monte Carlo framework was developed by Maretzki (2006) and Maretzki et al. (2007), that defined the main features of the present MCS model, notably the inclusion of actual bottom bathymetry and transect geometry, the use of stability analyses to estimate slope failure, and empirical equations to predict tsunami generation and impact. Although these key features are still part of the present MCS model, as will be reported in detail in this paper, many new improvements were made to this initial work, yielding important differences in both the MCS methodology and results (and hence conclusions) of the work. In particular, improvements were made in the estimation of peak horizontal accelerations, choice of sediment properties, inclusion of excess pore pressures in the analysis, slope stability analyses, evaluation of the statistics and return periods of tsunami runup, and estimation of tsunami propagation and nearshore breaking height. Hence, the Maretzki et al. work should thus only be viewed as an illustration of the potential for using a MCS approach to quantify tsunami hazards, while the present work provides both more realistic MCSs and results.

In the MCS model, the relationship between slope failure parameters and tsunami source characteristics is expressed based on empirical relationships developed as part of earlier numerical and experimental work, done mostly for idealized rigid slides (or slumps) of nearly semi-elliptical shapes, sliding down plane slopes (Grilli and Watts, 1999; Grilli et al., 2002; Enet et al., 2003; Grilli and Watts, 2005; Watts et al., 2005a; Enet and Grilli, 2005; Enet, 2006; Enet and Grilli, 2007). While this clearly constitutes an approximation with respect to actual slide dynamics, particularly for longer time scales of motion, numerical simulations, in which both rigid and deforming slides were compared, clearly showed that: (1) the short time behavior of a SMF (i.e., the slide early time kinematics), to a first-order, governs the key parameters of the tsunami source (e.g., such as the tsunami initial surface depression); (2) this early time behavior is best expressed by the magnitude of the initial slide acceleration, which itself mostly depends on slide density (geometry/volume) and bottom slope, and not on subsequent slide deformation (Haugen et al., 2005; Grilli and Watts, 2005; Watts et al., 2005a); (3) at such short time scales, slide deformation does not yet play a role on tsunami features, and by the time deformation (and slide break-up) occur, the slide is in deeper water and effects of deformation only provide small (second-order) changes to the main tsunami features; and (4) the importance of short time scales for tsunami generation, and hence short distances of slide motion, also justifies the approximation of a plane slope in numerical

simulations and experiments, rather than using the actual bottom geometry (here along a transect).

The two empirical equations used in the MCS model to predict initial tsunami amplitude based on SMF characteristics, are given later in the paper (Eqs. (18) and (19)). These equations were experimentally verified for rigid slides in two- (Grilli and Watts, 2005) and three-dimensions (Enet and Grilli, 2007), and also the basis for conducting a series of successful case studies of past landslide tsunamis (both by Grilli and co-workers, e.g., Watts et al., 2003; Day et al., 2005; Tappin et al., 2008; and by a few others). More details regarding the development and validation of these empirical relationships can be found in the above-listed references.

The new MCS model follows the basic flowchart shown in Fig. 2. The first step in the procedure consists in selecting a slide trial surface and corresponding bathymetry, sediment type and properties, and excess pore pressures, required to perform a slope stability analysis. Depending on sediment type, an appropriate pseudo-static limit equilibrium method is applied (i.e., Infinite Slope for cohesionless materials, and Modified Bishop's Method for cohesive materials). The seismicity is incrementally increased for various return periods (e.g., 50, 100, 150 yr…), to determine the minimum Peak Horizontal ground Acceleration (*PHA*) required for failure to occur, up to a maximum acceleration corresponding to an arbitrarily set 750 yr seismic return period. If the selected trial surface does not fail within this *PHA* range, this particular combination of slope parameters is deemed to be stable, and the model selects a new trial surface and repeats the process. Once failure is assessed, its size (length, width, thickness), depth, and other physical parameters are used in the empirical equations to estimate the generated tsunami elevation. If a wave occurs with an initial height greater than an arbitrary small 0.02 m elevation, a tsunami is deemed generated and the model estimates tsunami propagation (including shoaling, breaking, and arrival time) and runup levels.

Since it was prohibitive to perform tens of thousands of tsunami propagation simulations in the MCS model, as indicated before, coastal runup generated for each SMF tsunami source was also estimated by a semi-empirical approach, based on results of earlier tsunami propagation simulations by the lead author and co-workers (e.g., Grilli and Watts, 1999; Grilli et al., 2002; Grilli and Watts, 2005; Enet and Grilli, 2005; Enet, 2006). The rationale for this approach is, first, in all SMF tsunamis considered here, both failure and resulting tsunami source locations (i.e., SMF center of mass) are relatively close to shore. Additionally, both numerical and experimental work, as well as field observations (e.g., PNG), indicate that, unlike co-seismic tsunami sources, SMF tsunami sources and hence the runup they cause on nearby shores, is highly directional, in the sense that the

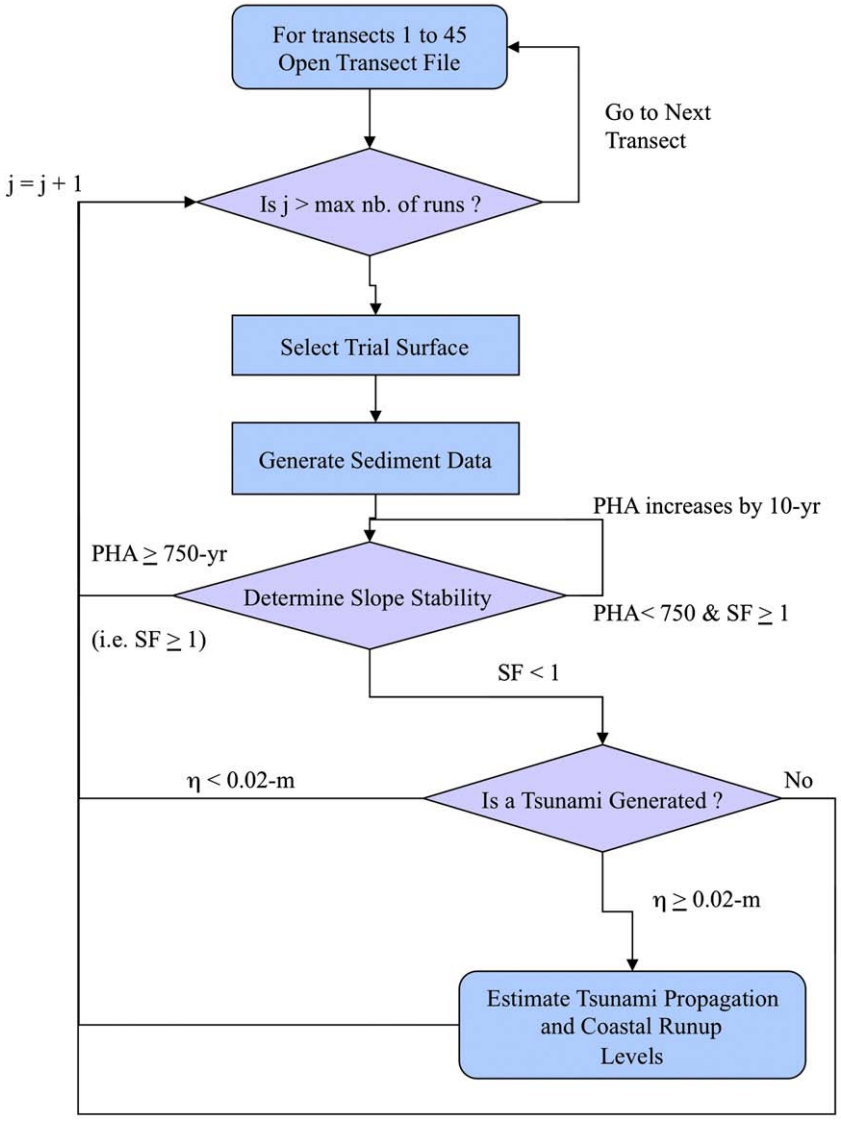

Fig. 2. Flowchart for the Monte Carlo Simulation (MCS) model used in this study.

largest waves (and runup) created by the SMF occur in (or near) the direction of SMF failure and wave elevation rapidly decreases laterally away from this direction (Enet and Grilli, 2007; and case studies listed above, as well as measured runup in known cases such as PNG; see, e.g., Fig. 4 in Tappin et al., 2008). In two-dimensional simulations of SMF tsunami generation and runup on a plane slope, Grilli and Watts (2005) found a nearly one-to-one correspondence between initial tsunami depression at the source and maximum runup; this correspondence was also found by Grilli et al. (2002) in three-dimensional simulations over a plane slope with a shallow shelf, and Enet and Grilli (2007) in similar three-dimensional experiments, for SMFs occurring close to the shoreline. In three-dimensional simulations over complex bottom topography, such as in the PNG case, this "correspondence principle" surprisingly is often nearly retrieved, just as if lateral energy spreading was approximately compensated by topographic focusing effects (for instance, with an initial 12-14 m depression estimated to be caused by the PNG slump initial characteristics, both simulations and observations show similar magnitude runup caused in the middle of the Sissano lagoon; Tappin et al., 2008).

Hence, in view of the directionality of the source and in the absence of more accurate results, to obtain a conservative order-of-magnitude estimate of coastal runup caused by each tsunamigenic SMF in the MCS model: (i) we first assume a main direction of tsunami propagation, in a random selected direction within a $+-5^\circ$ sector of the considered failed transect (usually nearly orthogonal to nearby shores); and (ii) we limit lateral spreading of coastal runup to an (arbitrary) $+-10^\circ$ angular variation from the selected main direction of propagation (Fig. 3). Maximum runup on the nearest shore is then assumed equal to the maximum tsunami depression at the source, and runup is then modulated alongshore. The natural shape of this alongshore modulation would be Gaussian as a first approximation (e.g., as seen in PNG runup observations; Tappin et al., 2008 Fig. 4), which is the choice made in the model (with a 95% width similar to the selected $+-10^\circ$ angular spreading; Fig. 3). [Note that recent three-dimensional laboratory experiments of (subaerial) landslide tsunami confirm such Gaussian-like alongshore runup variations (see Fig. 8 in Di Risio et al., 2008).] It should be stressed that the SMF tsunami source distance to shore, or the width of the shelf, does not directly affect the directionality of generated waves (in both onshore and offshore directions). However, significant local bathymetric features near the coast, such as a canyon (as off of the Hudson River), which are neglected in the MCS, could defocus (or focus) SMF tsunami waves, and such effects would be more prevalent the further away the tsunami source from the shore.

Fig. 4 shows various types of probability distributions known (or assumed) for the input parameters (e.g., depth to failure, sediment properties, etc…) and obtained for model outputs (i.e., factor of safety, initial tsunami amplitude, and runup). The use of log-normal and normal (Gaussian) input parameter distributions in the slope stability analyses yields a Weibull distribution of the resulting safety factor. The output of the slope stability analyses, with uniformly distributed angular displacement for rotational failures, yields a log-normal distribution for the initial tsunami amplitude, with a large bias towards small-amplitude tsunamis. The output of the initial tsunami amplitude and normally distributed propagation parameters (see details later) results in a log-normal distribution of runup for any given coastal point. The fact that the output probability distributions significantly differ from the input distributions is a result of the non-linearity of the MCS model.

2.2. Bathymetry and sediment properties

The bathymetry of the U.S. Northeastern continental shelf (NOAA, 2006) was mapped in ArcGIS-9, and 45 representative transects were selected and calculated in the GIS (Maretzki, 2006; Fig. 1). Transect locations were chosen such as to provide a representative sampling of the major geological features. It should be noted that, in sensitivity analyses (not reported here), the selected transect spacing was found sufficient to ensure a good convergence of MCS model results. Transects were discretized into a large number of points within the GIS and, for each transect point, a UTM (*Universal Transverse Mercator*) coordinate was assigned in conjunction with a depth below mean water. [Transect points were stored as (bathymetric) data files for use within the Monte Carlo model.] Transects are numbered from North to South (Fig. 1), with Transect #1 being in the vicinity of Cape Cod, MA and Transect #45 being located near the Southern end of the New Jersey coast.

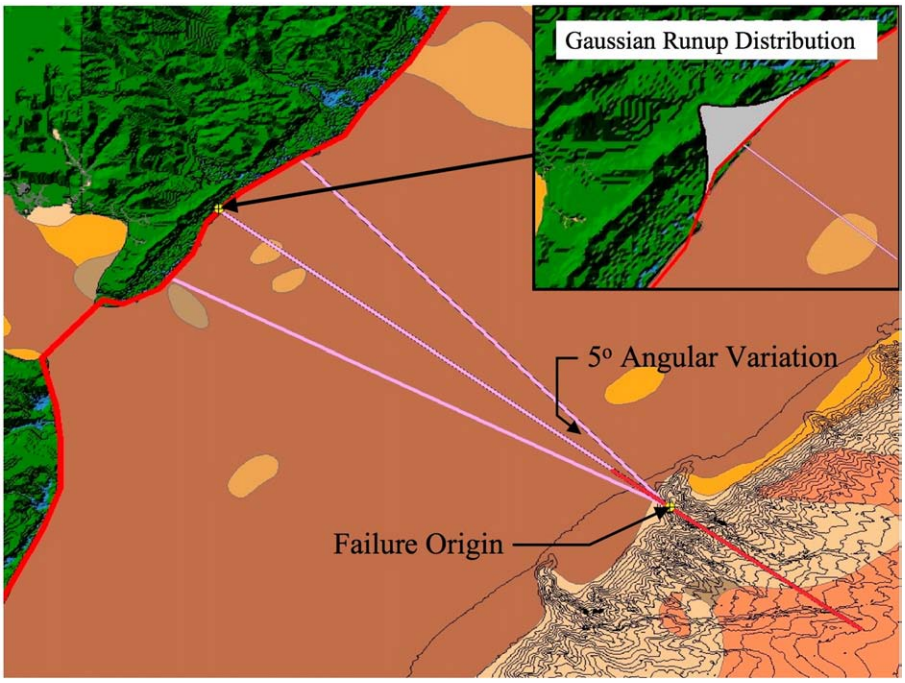

Fig. 3. Tsunami propagation picked within an angular spread from the failed transect direction, with insert of Gaussian distribution of coastal runup (within a $+-10^\circ$ sector).

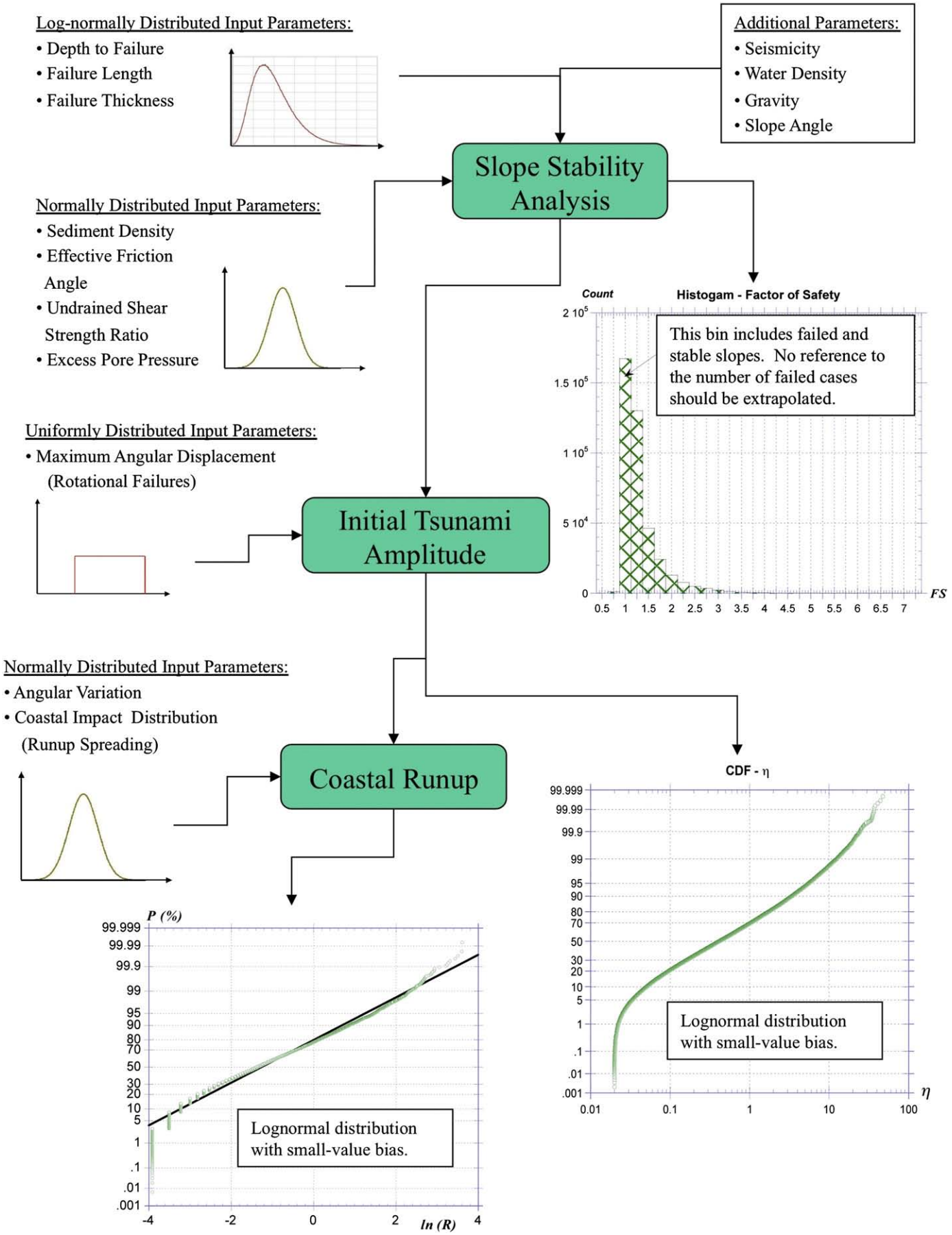

Fig. 4. Probability distributions in MCS model input parameters and key results (illustration of model non-linearity).

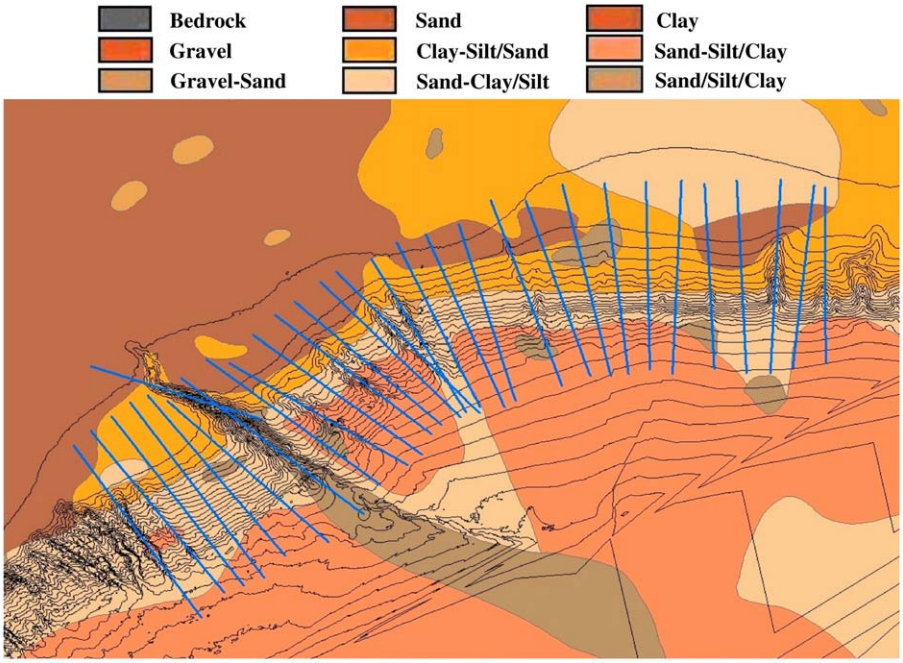

Fig. 5. Color-coded sediment types and topographic contours, represented in ArcGIS. Transects (45 blue lines) used in slope stability analyses are also shown. (For interpretation of the references to colour in this figure legend, the reader is referred to the web version of this article.)

The northeast U.S. shoreline contains many irregularities that cannot be considered in the MCS model, due to the simplified representations of tsunami propagation and runup. Therefore, Maretzki (2006) simplified the coastline into a multi-linear shape, by eliminating such irregularities (e.g., Long Island Sound). Doing so, a series of shoreline points (defined by latitudinal and longitudinal coordinates) was generated in ArcGIS-9 and for use in the tsunami propagation/runup part of the MCS model. The coastal points are numbered from 1–900, in the same manner as the transects: north to south from Cape Cod, MA to northern Delaware.

Surficial sediment properties were obtained from the Continental Margin Mapping (CONMAP) database (Poppe et al., 2005) and incorporated into ArcGIS-9 as well (Fig. 5). While the sediment found along each transect is not homogeneous laterally, it was assumed to be homogeneous vertically. Furthermore, the depth to bedrock, which is unknown within the region, was assumed to be greater than the maximum failure thickness selected in the model. This assumption is reasonably valid for open slopes; it may not be valid for some geological features such as canyon walls (e.g., Hudson River Canyon), which are typically steep and stable, due to shallow bedrock features.

Each identified sediment type was assigned both a range of physical properties and geographic boundaries (defined in UTM coordinates). These were exported as data files for use within the MCS model. For each randomly selected failure point coordinates along a given transect, a corresponding sediment type is thus found, for which randomly selected physical and strength properties are assigned (within the specified sediment's ranges). It should be noted that sediment properties in the study area, such as type, bulk density, strength, and excess pore pressure, yield the greatest uncertainty in the analysis, due to the lack or paucity of geotechnical borings along the U.S. Northeastern Continental Shelf. [The only publicly available boring data for this region is provided by the Ocean Drilling Program database (ODP, 2008), for only three bore holes in our area (Sites 1071, 1072, and 1073), all of which are located in the same region along the Hudson Apron (Leg 174A).] Because of this, information on surficial

Table 2
Sediment classification and strength parameters used in MCS model.

USGS sediment description[a]	GIS sediment layer generalized classification[b]	Effective stress angle of internal Friction [ϕ']	Undrained shear strength ratio [s_u/s'_v]	Assumed failure type
Gravel	Gravel	40–44°	–	Translational
Sand	Sand	32–36°	–	Translational
Gravelly *sand*	Gravel–sand	36–40°	–	Translational
Silty *sand*	Clay–silt/sand (type I)	30–34°	–	Translational
Clayey *sand*	Clay–silt/sand (type II)	28–32°	–	Translational
Sand with silt and clay	Sand/silt/clay (type I)	28–32°	–	Translational
Silt	Sand–clay/silt (type I)	–	0.18–0.22	Rotational
Sandy *silt*	Sand–clay/silt (type II)	28–32°	–	Translational
Clayey *silt*	Sand–clay/silt (type III)	–	0.19–0.23	Rotational
Silt with sand and clay	Sand/silt/clay (type II)	–	0.17–0.21	Rotational
Clay	Clay	–	0.20–0.24	Rotational
Sandy *clay*	Sand–silt/clay (type I)	–	0.18–0.22	Rotational
Silty *clay*	Sand–silt/clay (type II)	–	0.19–0.23	Rotational
Clay with sand and silt	Sand/silt/clay (type III)	–	0.19–0.23	Rotational

[a] Predominant grain-size is italicized, which is used to merge similar sediment into a simplified and usable ARC-GIS 9 layer, with generalized sediment classifications.
[b] To account for sediment variability within the simplified ARC-GIS 9 layer, each USGS classification is separated by "type" with a uniform probability of occurrence within the MCS model.

sediments from CONMAP was used instead, to construct uniform sediment profiles within the study region.

Based on such sediment classifications, effective stress friction angles [ϕ'], ranging from 28° to 44°, were used for coarse-grained sediments, and undrained shear strength ratios [S_u / σ'_v], ranging from 0.17 to 0.24, were used for fine-grained sediments (Table 2). Vertical effective stresses [σ'_v] were calculated, assuming no overpressure (i.e., normally consolidated conditions), and the increase in bulk density with depth was assumed to be similar to that of data collected in ODP Leg 174A. The sediment data, together with bathymetric and topographic data, was then used to create a series of additional GIS layers in ArcGIS-9 (Fig. 5).

2.3. Seismicity

Seismicity was characterized along transects based on a United States Geological Survey database (USGS, 2007), which was developed to provide an estimate of peak horizontal ground (bedrock) acceleration [*PHA*], for any location of the continental and coastal U.S. (defined by its latitude and longitude) and for nineteen annual rates of exceedance (Fig. 6). These seismic hazard maps consider onshore and offshore faults, subduction zones, and historical background seismicity, and are assumed to be accurate within the longitudinal extent of the U.S. Exclusive Economic Zone (to 65-degrees W longitude; Harmsen, USGS 2008, personal communication). The study region considered in the MCS analysis falls well within this zone of applicability; hence, the USGS database is deemed sufficiently accurate to estimate the *PHA* in the study area. In the model, the latter was discretized over a 0.1°×0.1° grid and all cells representing inland locations were removed (Maretzki, 2006). To improve the MCS efficiency, polynomial curve fits of ln(*PHA*) as a function of the probability of exceedance were made for each cell on the transects, using USGS data.

Once a trial failure surface is selected along a transect in the MCS model, the curve fit for that location is used to determine *PHA* values, for different annual rates of exceedance (e.g., for 50, 60, 70,…, 500 yr). Increasing values of *PHA* are thus applied in the slope stability analysis, until failure occurs or the annual rate of exceedance exceeds 750 yr. It is assumed that the trial surface will fail for any *PHA* greater than the minimum value found to cause failure. Therefore, for a 100 yr seismic triggering event, all failures with a minimum *PHA* of 100 yr or less are included within the statistical analysis. Likewise, for a 500 yr seismic triggering event, all the 100 yr seismic data is included, along with additional failures with a minimum *PHA* corresponding to a

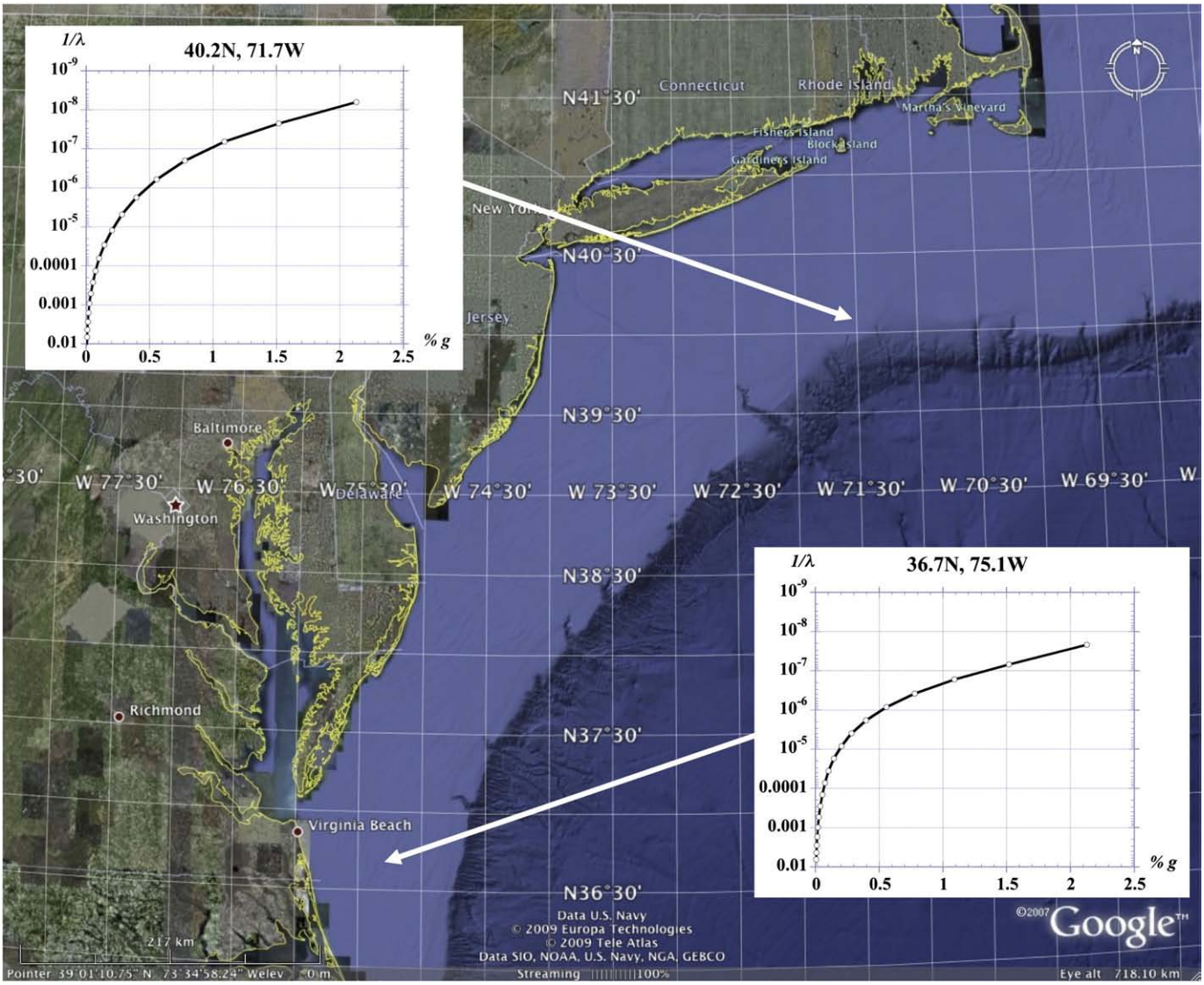

Fig. 6. Typical peak horizontal acceleration probability distribution, at two locations (0.1° grid cell) within the study area; probability is expressed as an annual probability of exceedance 1 / λ. The curves are polynomial fits of the probability to the log of the acceleration data from USGS maps (2007).

return period less than 500 yr. With this methodology, the probability for a tsunamigenic slope failure to occur in our study area, and that of related tsunami hazard, can be assessed more accurately than in our earlier MCS approach (e.g., Maretzki et al., 2007).

2.4. Slope stability analyses

In the MCS model, slope stability is assessed by applying two pseudo-static limit equilibrium methods, depending on the type of sediment found along each transect, and hence likeliest failure mechanism: (i) translational failures (i.e., slides or infinite slope failures) for coarse-grained sediments; and (ii) rotational failures (i.e., slumps) for fine-grained sediments. In both cases, failure is assumed to be triggered by the *PHA* generated by an earthquake, as determined from the exceedance probability distribution for the considered location (Fig. 6), in combination with excess pore pressures (above hydrostatic conditions; see next section). In the stability analyses, the earthquake is assumed to cause a pseudo-static horizontal inertial force (in view of the relatively short duration of seismic ground motions on the order of 10 s), proportional to the total sediment mass, applied to the center of mass of the selected tentative failure volume and oriented in the downslope direction.

In seismic analyses, maximum *PHA* values are typically reduced to account for various natural damping mechanisms, by applying a seismic coefficient k defined as [0,1] *PHA* / g, with g the gravitational acceleration (typical values are 50 to 85% *PHA* / g; e.g., Terzaghi, 1950; Seed, 1979). However, bedrock ground motions can be amplified significantly as they propagate through soft sediments towards the seafloor. Considering the lack of detailed information about sediment stratigraphy, depth to bedrock, and sediment properties that would be necessary for a thorough site response analysis, in our analyses, it was assumed that the effects of reducing *PHA* and the subsequent motion amplification would cancel each other, and thus a value of k equal to the *PHA* / g was used in MCSs. Furthermore, due to the relatively small *PHA* magnitude within the region (typically less than 0.02 g), extremely large amplification (when combined with the reduction for the pseudo-static coefficient) would be required to create a noticeable difference in our pseudo-static analysis calculations of the factor of safety.

2.4.1. Infinite slope method

This method is used to assess the stability of translational failures of homogeneous cohesionless slopes using effective stress parameters. The failure plane is assumed to be at relatively shallow depth and parallel to the slope face, which implies that slide length $l \gg T$, the slide thickness perpendicular to the failure plane (Fig. 7). In this procedure, one expresses the equilibrium of gravity, seismic, and frictional forces, with the moment equilibrium being implicitly satisfied. Summing the forces parallel and perpendicular to the failure plane yields,

$$S = W' \sin\beta + kW\cos\beta \tag{1}$$

$$N = W' \cos\beta - kW\sin\beta \tag{2}$$

where $W = \rho_s g V$ is the total weight of the failed mass, $W' = (\rho_s - \rho_w) gV$ is the buoyant weight, β is the seafloor slope angle, and $V = lT$ is the slide volume per unit width, with ρ_s and ρ_w the sediment bulk and water density, respectively. The effective shear and normal stresses per unit width acting on the failure plane are then calculated as,

$$\tau_d = \frac{S}{l} = Tg((\rho_s - \rho_w)\sin\beta + k\rho_s\cos\beta) \tag{3}$$

$$\sigma' = \frac{N}{l} = Tg((\rho_s - \rho_w)\cos\beta - k\rho_s\sin\beta). \tag{4}$$

To account for any change in pore pressure above hydrostatic conditions (e.g., from initial excess pore pressure, seismic activity, etc…), a stress Δu defined as,

$$\Delta u = R_u(\rho_s - \rho_w) gT\cos\beta \tag{5}$$

is subtracted from the effective normal stress σ', with R_u a stress reduction factor, whose meaning and value are detailed in the next section.

Hence, the limit equilibrium equation expressing the slope factor of safety reads,

$$FS = \frac{c' + (\sigma' - \Delta u)\tan\phi'}{\tau_d} \tag{6}$$

which, for cohesionless sediment ($c' = 0$) and using Eqs. (3)–(5), reduces to,

$$FS = \frac{(s-1)(1-R_u) - ks\tan\beta}{(s-1)\tan\beta + ks}\tan\phi' \tag{7}$$

with $s = \rho_s / \rho_w$ the sediment specific density.

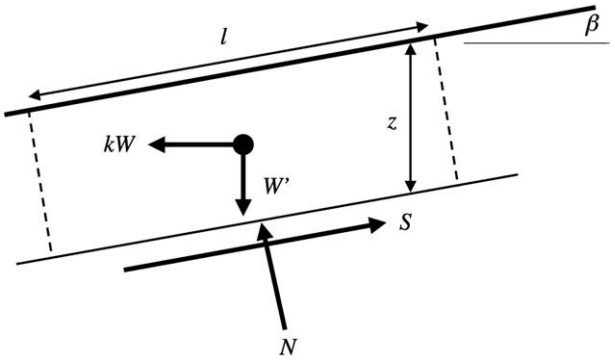

Fig. 7. Forces acting on a translational slope failure (infinite slope), including a pseudo-static horizontal force to simulate seismic loading.

2.4.2. Modified Bishop Method

This method is used to assess slope stability for deep rotational failures (i.e., slumps) occurring in fine-grained cohesive materials, under undrained loading conditions. The failure surface is approximated by a circular cylinder, and the region between this surface and the slope is divided into vertical slices (Fig. 8a). Both moment and vertical force equilibrium are expressed using total stress strength parameters.

In the assumed geometry, we denote r the failure circle radius and, for each slice i: a_i is the failure plane angle at the base of each slice, k, W_i and W_i' are defined as in the infinite slope method, N_i is the normal force, $S_i = \tau_i \Delta l_i$ the shear force, with the width of each slice Δl_i, being an equal fraction of the failure circle arc length (Fig. 8b). Expressing the equilibrium of the moment of forces about the center of the failure circle, for slices $i = 1,\ldots, I$, we find,

$$r\sum_{i=1}^{I}\left(\frac{\tau_i \Delta l_i}{FS} - W_i'\sin\alpha_i - kW_i\frac{d_i}{r}\right) = 0 \tag{8}$$

in which the shear force is divided by the factor of safety FS. The seismic lever-arm d_i can be further expressed in terms of the radius of the failure circle as,

$$d_i = r\cos\alpha_i - \frac{\bar{h}_i}{2} \tag{9}$$

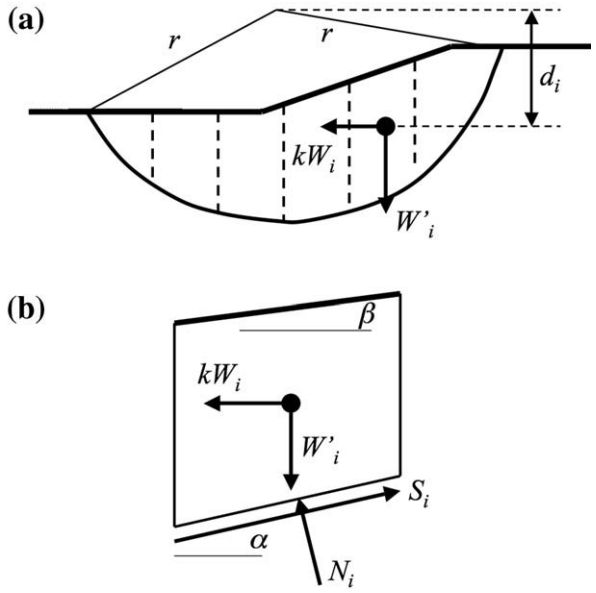

Fig. 8. (a) Rotational slope failure in the Bishop Method, with an additional horizontal seismic force. (b) Free body diagram of an individual slice.

where $\bar{h}_i$ is the average slice height. Substituting Eq. (9) into Eq. (8), expressing the shear stress τ_i as a function of the undrained shear strength, and solving for *FS*, we find,

$$FS = \frac{\sum_{i=1}^{I} S_{u_i}\,\Delta l_i}{\sum_{i=1}^{I}\left(W'_i \sin\alpha_i + kW_i\left(\cos\alpha_i - \frac{\bar{h}_i}{2r}\right)\right)} \tag{10}$$

where S_{u_i} is the undrained shear strength of the sediment, for each slice.

3. Excess pore pressures

There is some evidence for the presence of excess pore pressures (i.e., above hydrostatic equilibrium conditions), along localized regions of the Hudson Apron (ODP Leg 174A, Site 1073), likely due to weak sandy drainage layers (Locat et al., 2003). Although these drainage layers are not believed to extend over our entire region of study, their distribution is not fully known. Pore pressures due to poor drainage layers, together with other pore pressures that could be generated as a result of seismic activity, greatly influence slope stability analyses, by causing a reduction in shear strength of the sediment. Hence, such a reduction was incorporated into the effective stress slope stability analyses performed within the MCS model.

Since there is no established method for calculating how much pore pressure (above hydrostatic) is generated during seismic activity, a stress reduction factor R_u is applied during simulations, to represent both the unknown initial conditions (overpressures related to drainage) and seismic pore pressure generation. This stress reduction factor is used to calculate the change in pore pressure above hydrostatic expressed by stress Δu in Eq. (5). Values of R_u are randomly selected between 0 and 1 during MCS simulations, using a Gaussian distributed random number $\Re$ (0 mean and 0.25 standard deviation), and semi-empirical equations depending on the failure type (translational, rotational), ϕ', and β. The latter equations are in part based on the subsurface investigation by Locat et al. (2003), but contain an additional coefficient *e*, whose value was empirically adjusted, in order for MCS results to closely approximate known failure type distributions within the region (i.e., frequency of failure type, from Booth et al., 1993).

Specifically, for rotational failures, we define,

$$R_{ur} = \Re r_r + \varepsilon \tag{11}$$

with the limits: $0 \le R_{ur} \le r_r$ and,

$$r_r = 1.01 - 0.09\beta \tag{12}$$

the maximum value of stress reduction calculated by Locat et al. (2003), for an undrained shear stress ratio $S_u/\sigma'_{vo} = 0.2$ prior to the occurrence of slope instability (applicable to most normally consolidated marine sediment; Ladd and Foote, 1974). For rotational failures, the best fit of the empirical coefficient is found to be $\varepsilon \cong 0.35$. With this value, Eqs. (11) and (12) yield, through the entire set of MCS trials for all the transects, a nearly Gaussian R_{ur} distribution (not shown), with minimum of 0, maximum of 0.96, mean of 0.38 and standard deviation of 0.16.

For translational failures, a similar approach is followed, by defining,

$$R_{ut} = r'_t + \alpha_t(r_t - r'_t) \quad \text{with} \quad \alpha_t = \Re + \varepsilon \tag{13}$$

$(-1 \le \alpha_t \le 1)$, and,

$$r'_t = 0.9 - 0.03\beta \tag{14}$$

defined as 90% of the pore pressure required to fail the slope (for a given β), under static conditions and with an effective friction angle of $\phi' = 28°$ (the lowest value that is considered within the MCS model). [Eq. (14) is easily derived as $r'_t = 0.9R_{ut}$ from Eq. (7), when solving it for R_{ut} and assuming $FS = 1$, $k = 0$, and $\tan\beta \cong \beta$ for small angles.] Similarly, we define,

$$r_t = 0.991 - 0.033\beta + 0.0003\phi' \tag{15}$$

as 99% of the stress reduction required for static failure of the slope. The first two terms in Eq. (15) are similar to Eq. (14) (except for a 0.99/0.9 factor), but the last term represents an empirical correction that accounts for changes in effective friction angle of the sediment.

For translational failures, the best fit of the empirical coefficient is found to be $\varepsilon \cong 0.5$. With this value, Eqs. (13)–(15) yield, through the entire set of MCS trials for all the transects, a nearly Gaussian R_{ut} distribution (not shown), with minimum of 0 (but almost no values between 0 and 0.5), maximum of 0.99, mean of 0.82 and standard deviation of 0.09.

As mentioned, using Eqs. (11)–(15) and the calibrated values of ε (0.35 and 0.5), we will show in the section on MCS model validation, that failure parameter distributions are in reasonable agreement with field observations by Booth et al. (1993) and Chaytor et al. (2007). In view of the near absence of data and information on excess pore pressure in the region, this agreement can be counted among the success of the present study.

3.1. Failure width

Once a failure has been identified in the MCS model to occur along one of the transects, its lateral extent must be determined. Due to the uniqueness of each site and the variability within the sediment distribution, there is no reliable method for accurately (and automatically) determining the lateral extent of a slope failure. In their landslide tsunami simulation work, Watts et al. (2005a) estimated that, based on published field observations, the width of translational failures (w_t) was approximately 25% of their length (l) and the width of rotational failures (w_r) was approximately equal to their length (see Watts et al. 's paper for references). These empirical values of w_t and w_r are used in the MCS model as a basis for estimating

failure width; to account for uncertainty, however, we allow for a random ±20% variability as,

$$w_t = 0.1(2 + \Re)l \tag{16}$$

$$w_r = 0.4(2 + \Re)l \tag{17}$$

where $\Re$ is a random variable, uniformly distributed between 0 and 1.

Finally, a maximum limit to the failure width was set, based on the distribution of known failures by Booth et al. (1993) and Chaytor et al. (2007), to ensure that failure widths selected in the MCS model would not be unrealistic for the region.

3.2. Tsunami generation and runup

As discussed before, for every failure identified in the slope stability model, an initial tsunami characteristic amplitude η_o is calculated using semi-empirical equations (developed for translational and rotational failures, based on two- and three-dimensional numerical simulations; Grilli and Watts, 2001; Grilli et al., 2002; Grilli and Watts, 2005; Watts et al., 2005a). For landslide tsunamis, η_o is defined as the maximum depression of the free surface above the submarine landslide geometrical center and given by,

$$\eta_{oT} = S_{oT}(0.0574 - 0.0431\sin\beta)\left(\frac{T}{l}\right)\left(\frac{l\sin\beta}{d}\right)^{1.25}\left(1 - e^{-2.2(s-1)}\right)\left(\frac{w}{w + \lambda_{oT}}\right) \tag{18}$$

$$\eta_{oR} = S_{oR}\left(\frac{0.131}{\sin\beta}\right)\left(\frac{T}{l}\right)\left(\frac{l\sin\beta}{d}\right)^{1.25}\left(\frac{l}{r}\right)^{0.63}(\Delta\Phi)^{0.39}(1.47 - 0.35(s-1))(s-1)\left(\frac{w}{w + \lambda_{oR}}\right) \tag{19}$$

for translational and rotational failures, respectively, with d the depth below sea level above the center of the failed mass, w the failure width, $(\Delta\Phi, r)$ the maximum angular displacement and radius of a rotational failure (see Fig. 9), S_{oR} and S_{oT} the characteristic distance of motion for translational and rotational and failures,

$$S_{oT} = \frac{\pi}{2}l(s+1) \tag{20}$$

$$S_{oR} = \frac{r\Delta\Phi}{2} \tag{21}$$

respectively, and the characteristic tsunami wavelength,

$$\lambda_{oT} = \sqrt{\frac{\pi l d(s+1)^2}{2\sin\beta(s-1)}} \tag{22}$$

$$\lambda_{oR} = \sqrt{rd\frac{(s+1)}{(s-1)}} \tag{23}$$

respectively. [Note, the last terms in Eqs. (18) and (19) express changes in characteristic tsunami amplitude due to three-dimensional lateral energy spreading, validated using Grilli et al. (2002) model.]

As also discussed before, the maximum runup for each particular slope failure is estimated as $R \approx \eta_o$, according to the "correspondence principle" (with η_o given by Eqs. (18) or (19) depending on failure type). The main direction of tsunami propagation is assumed to occur near that of the failed transect, with some randomness added within an arbitrary ±5° angular variation (Fig. 3). Maximum runup R occurs on the coast in this direction, and runup is then modulated alongcoast assuming a Gaussian shape and an angular spreading of ±10° on either side of the maximum runup location (Fig. 3 insert). Runup values, corresponding to each failure and transect, are tabulated together for the 900 points describing the idealized Northeastern U.S. Coastline (Fig. 3). Once all MCSs are completed, runup statistics are calculated for each coastal point. This will be detailed later.

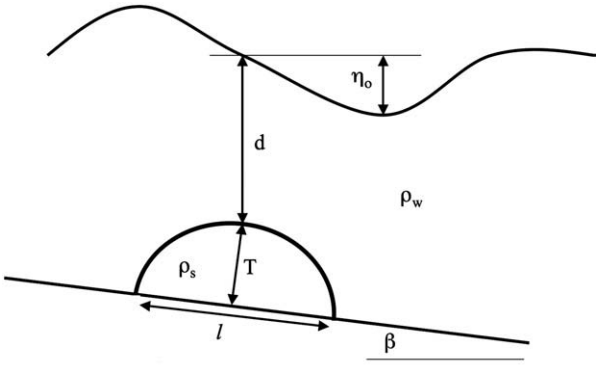

Fig. 9. Sketch for the generation over a slope of angle β, of a tsunami with characteristic amplitude η_o, by a typical SMF slide of length l, thickness T, average depth d, and density ρ_s.

3.3. Tsunami breaking height estimate

The tsunami breaking height H_b was estimated for each coastal point, within each region of elevated risk identified in the MCS model (defined later), using long wave theory (e.g., Dean and Dalrymple, 1984), with some additional assumptions: (i) no refraction is considered, hence tsunami wave rays are assumed to be straight, in the main direction of propagation (along coordinate x), from the point of origin (i.e., the SMF source center of mass) to the shore; (ii) similar to the simplification of the coastline geometry, the shoreface bathymetry is idealized as a plane mild slope (1:35), extending from shore to a water depth equal to 65 m or 65% of the water depth at the top of continental slope, whichever is largest; and (iii) the continental shelf bathymetry is assumed to vary linearly from the toe of the shoreface to the top of the continental slope.

Wave height variation as a function of depth is classically obtained from energy flux conservation as (o indices indicate deeper water quantities),

$$\overline{E}c_g \approx \frac{1}{8}\rho g H_o^2\sqrt{gh_o} = \frac{1}{8}\rho g H^2\sqrt{g(h+H)} \tag{24}$$

with $\overline{E}$ the time-averaged wave energy, $h_o = d$ the initial water depth at the landslide location, and $c_g = c$ the long wave group velocity, equal to the phase velocity (note the nonlinear correction of phase speed in the right hand side of Eq. (24), in shallower water, because of the large anticipated tsunami height near the shore). Simplifying, we get,

$$\frac{H}{H_o} = \left[\frac{h_o}{h+H}\right]^{1/4} \tag{25}$$

which is similar to Green's law, except for the nonlinear correction. [Eq. (25) can be solved iteratively, to provide $H_i(x)$ as a function of $h_i(x)$, at a series of points $i = 1,\ldots, I$, spaced Δx along the direction of tsunami propagation.]

For long waves, breaking is assumed to occur, at $x = x_b$, when the ratio of wave height to local depth $H_b/h_b = \kappa$, the breaking index (taken equal to 0.8 in the model for a mildly sloping bottom). Therefore, Eq. (25) yields the breaking depth,

$$h_b = \left[\left(\frac{H_o}{\kappa}\right)^4\frac{h_o}{1+\kappa}\right]^{1/5} \tag{26}$$

and $H_b = \kappa h_b$, with x_b obtained from the nearshore bathymetry.

3.4. Tsunami travel time estimate

Tsunami travel times t_0 can be estimated, over the idealized bottom topography, from the SMF source ($x = 0$) to the breaking point

($x=x_b$), based on the same long wave approximation, by integrating $1/c$ over space (with $c=(g(h+H))^{1/2}$ and $H(h(x))$ given by Eq. (25)); and similarly from the breaking point to shore ($x=x_0$), assuming a local wave height $H=\kappa h$ and a constant bottom slope $s=h_b/(x_0-x_b)$ in the surfzone. After simple analytical developments we find,

$$t_0=\sum_{i=1}^{I}\frac{\Delta x}{\sqrt{g(h_i+H_i)}}+2\left(\frac{x_0-x_b}{gs(1+\kappa)}\right)^{1/2}. \tag{27}$$

An average arrival time $\bar{t}_0$ was calculated for all tsunamis reaching a given coastal point, as the average of travel times weighted by their respective runup.

3.5. Results of Monte Carlo simulations

The data returned from the MCS model yields both deterministic physical sediment and SMF properties, for each pseudo-static analysis and tsunami generation and, for each coastal point, an ensemble of tsunami runups, breaking heights, breaking point locations, and tsunami travel times.

This simulated data must be subjected to a statistical analysis, before any meaningful tsunami hazard and risk assessment can be made. This is detailed in Section 3, with validation given in Section 4.

4. Statistical analysis

4.1. Principle

An accurate estimate of tsunami hazard requires a proper statistical analysis of MCS results. However, owing to the vast amount of simulated data, it can be difficult verifying that the applied methodology produces realistic results. Hence, each step in the analysis must thus be thoroughly understood and validated.

For lack of better guidance, the methodology (and terminology), used here to assess tsunami hazard along the Upper U.S. East Coast, is consistent with other standard methods used, e.g., by U.S. Federal agencies to assess similar hazards (e.g., NOAA for hurricanes, USGS for earthquakes, and FEMA for floods). This ensures that resulting tsunami hazard maps are consistent with other similar hazard maps, and can thus be interpreted in the same manner.

While the definition of return periods for earthquakes and induced *PHA* is well understood, one must clearly define the resulting 100 yr and 500 yr tsunami events, leading to coastal impact (i.e., runup and inundation) of a similar return period. The latter is the key effect of SMF tsunamis, whose hazard this work aims at quantifying. However, there is no simple correlation between these two types of return periods (i.e., a 100 yr earthquake at a given location does not trigger a 100 yr tsunami). A given earthquake may or may not trigger a SMF tsunami, but when it does, the tsunami magnitude and coastal impact depend upon a complex set of parameters, nonlinear physical processes, and local conditions, which we have attempted to describe in the MCS model discussed before.

Consistent with the method used, e.g., for storm surge analysis, coastal runup (and inundation) caused by a tsunami is defined to have a return period (or recurrence interval) of X years, if its magnitude is such that it is equaled or exceeded once on average every X years. The reciprocal of the return period is the probability that tsunami runup or inundation be equaled or exceeded in any given year. Using the same definition, an X year tsunami runup (e.g., 100/500 yr) thus has a $1/X$ annual probability (e.g., 1/0.2%) of being equaled or exceeded in any single year. It should be stressed that this return period definition does not imply that the X year tsunami will occur once over the next X years; instead, this will only be true in average, over a much longer time span than X (large number theorem).

4.2. SMF return period

Prior to performing statistical analyses of MCS coastal data, one must define the return period of tsunamigenic slope failures (SMF) caused by a given seismic triggering ground acceleration (e.g., for a 500 yr earthquake), including the possibility that such a *PHA* will not trigger any failure. This is achieved by calculating the joint probability of occurrence P_{SMF}, of a Y yr *PHA* (of probability $P_{PHA}=1/Y$) and a tsunamigenic SMF (of probability P_f) as,

$$P_{SMF}=P_{PHA}P_f \tag{28}$$

with,

$$P_f=\frac{n}{N} \tag{29}$$

where n is the total number of tsunamigenic slope failures identified in the MCS model, given a Y yr (e.g. 100/500 yr) *PHA*, for a total of N trials across the study area. [Note, only failures that resulted in tsunami amplitudes greater than 0.02 m were counted in n. A variety of threshold values were tested, to determine which tsunami amplitude should be considered significant regarding coastal impact. Thus, increasing the threshold from 0.02 m to 1.0 m resulted in less than a 5% difference in runup. Considering amplitudes less than 0.02 m, however, resulted in a significant increase in n, yielding a large bias of runup distributions towards the small values.]

4.3. Number of trials and model convergence

Due to its probabilistic nature, each time the MCS model is run, slightly different results and distributions are obtained (e.g., for tsunamigenic slope failures size, geometry, and types (i.e., translational or rotational), tsunami runups, etc…), and results also depend upon the number N of trials used, which must be large enough to ensure that output distributions are both realistic and converged, as compared to some known distributions. To ensure a realistic geometry of slope failure, constraints were imposed based on distributions of failure size and type, obtained from field campaigns within the study region (Booth et al., 1993). Regarding model convergence, Nowak and Collins (2000) indicate that the distribution of all possible MCS results can be characterized by a degree of variation (expressed in terms of a coefficient of variation *CoV*). Based on this, the annual-probability P_{max}, of the maximum return period that can be estimated in a probabilistic model, for N simulations, is given by,

$$P_{max}=\frac{1}{(NCoV^2)+1}. \tag{30}$$

A coefficient of variation $CoV=10\%$ was assumed in this study (Nowak and Collins, 2000), and (after some trials) we used 15,000 simulations for each of 45 transects, hence, $N=675{,}000$. Therefore, from Eq. (30), $P_{max}=0.000148$ (or a 0.015% annual-probability event), and the maximum return period that can accurately be estimated is 6750 yr. Note, this maximum does not refer to any specific event (e.g., tsunamigenic SMF), but rather is the limit of accuracy of the statistical analysis: if any annual probability is less than P_{max} then the number of trial surfaces in the MCS model must be increased to ensure convergence, given the selected *CoV* value.

4.4. Runup statistics

Coastal runup statistics can now be generated based on the return period of the tsunamigenic slope failure ($1/P_{SMF}$), which is in general different from that Y of the *PHA*. Accordingly, it is expected that the runup data generated at each coastal point, for a given tsunamigenic

slope failure return period ($1/P_{SMF}$), will contain on average a tsunami runup corresponding to this event. [For example, runup data at each coastal point for a $1/P_{SMF}=2500$ yr tsunamigenic SMF is expected to contain on average one 2500 yr tsunami runup event, and five 500 yr tsunami runup events.] The design tsunami for a given return period X (e.g., 100 yr) is defined as the event that causes a tsunami runup with annual probability of exceedence $P_X=1/X$ (e.g., 1%) at each coastal point; hence, this runup is expected to be equaled or exceeded once, on average, during a X yr period.

To calculate the design tsunami runup for a given coastal point, runup values collected from all tsunamigenic SMFs affecting this particular coastal point are first sorted in descending order (from 1 to M, where M is the number of runup data for that coastal point, with magnitudes greater than 0.02 m). The mth largest runup value is then selected such that $m=(0.01)\,M$. The design runup is then selected as the xth largest runup value such that,

$$x=\frac{P_X}{P_{SMF}}m \tag{31}$$

Fig. 10, and the example below, illustrate the application of this method to Coastal Point 700 in our MCS.

Example. For Coastal Point 700 (along the New Jersey coastline), there are $M=5963$ collected tsunami runups corresponding to the SMFs identified in the MCS model. For $N=675{,}000$ simulations (as discussed before) the MCS model identifies $n=104{,}637$ tsunamigenic SMFs, for a *PHA* corresponding to the $Y=500$ yr earthquake ($P_{PHA}=1/Y=0.2\%$ annual probability). From Eq. (29), the probability of a tsunamigenic SMF is: $P_f=\frac{n}{N}=\frac{104{,}637}{675{,}000}=0.15501$.

Therefore, the joint annual probability of a tsunamigenic SMF (Eq. (28)) is:

$$P_{SMF}=P_{PHA}\cdot P_f=0.002\cdot 0.155 \approx 0.0003 \text{ (or a 3350 yr. return period).}$$

Thus, runup data collected for each coastal point contains up to a 3350-yr tsunami runup event. [Note, results of the MCS model are within the acceptable CoV (assumed to be 10%), and hence converged, since $P_{SMF}>P_{max}=0.000148$ from Eq. (30).]

Once runup data for point 700 has been ranked in descending order, Eq. (31) indicates, the $x=60$th point (1%-percentile point) represents the 3350 yr runup event (since $P_X=P_{SMF}=0.03\%$ annual-probability tsunami), or 11.12-m (Fig. 10), and the $x=1987$th point is the 100 yr runup event (1% annual-probability tsunami), or 0.7 m; similarly, the $x=398$th point is the 500 yr runup, or 3.91 m. Furthermore, by definition, it is expected that on average six 500-yr tsunamis and thirty-three 100-yr tsunamis should be contained within the entire coastal runup data set.

It is important to note that these are global hazard levels and they do not consider the nearshore bathymetry or shoaling effects. Detailed tsunami modeling is required to determine the local-scale hazard levels, which may yield up to a significant increase in inundation.

5. Validation of Monte Carlo simulation model

The relevance of probability distributions specified or generated in the MCS model, for each input and output geometric or physical parameter (e.g., slide depth, length, etc…), is the key to the accuracy of tsunami hazard assessment, as improper distribution functions will

Results for Coastal Point 0700

Max Seismic Return Period 500 years
Tsunamigenic Slope Failure Return Period 3350 years

Location: Lat 39.6 Lon -74.21

Total Number of Data Points 5963

0.03%-annual-chance of being exceeded (3,350 year tsunami) (z = 60)

0.2%-annual-chance of being exceeded (500 year tsunami) (z = 398)

Runup

39.83	16.1	13.03	10.41	9.28	8.31	7.55	6.98	6.59	6.02	5.55	5.27	5.04	4.76	4.57	4.37	4.12	3.94
36.38	15.96	13.03	10.34	9.26	8.3	7.52	6.95	6.58	6.01	5.53	5.26	5.04	4.75	4.57	4.37	4.12	3.93
34.38	15.65	12.67	10.23	9.25	8.27	7.49	6.93	6.58	5.98	5.51	5.24	5.04	4.74	4.55	4.36	4.1	3.93
32.27	15.48	12.62	10.07	9.19	8.27	7.47	6.91	6.56	5.97	5.49	5.23	5.03	4.74	4.55	4.34	4.09	3.93
31.41	15.2	12.35	10.04	9.04	8.23	7.47	6.89	6.53	5.96	5.49	5.23	5.02	4.74	4.54	4.32	4.09	3.93
28.35	15.16	12.01	9.96	9	8.2	7.41	6.89	6.52	5.93	5.48	5.22	5.01	4.71	4.54	4.31	4.09	3.92
24.25	15.07	11.73	9.93	8.95	8.09	7.41	6.85	6.49	5.91	5.48	5.2	5	4.69	4.52	4.3	4.08	3.91
23.19	15	11.66	9.92	8.91	8.08	7.38	6.84	6.48	5.89	5.48	5.18	5	4.69	4.51	4.3	4.08	3.91
22.91	14.81	11.65	9.86	8.78	7.96	7.33	6.82	6.48	5.86	5.47	5.17	4.98	4.68	4.5	4.28	4.08	3.9
20.17	14.76	11.63	9.84	8.74	7.93	7.26	6.8	6.48	5.83	5.46	5.16	4.96	4.68	4.49	4.27	4.06	3.87
19.52	14.52	11.54	9.82	8.73	7.91	7.26	6.79	6.47	5.8	5.44	5.15	4.94	4.68	4.48	4.25	4.04	3.86
19.49	14.49	11.32	9.74	8.68	7.84	7.25	6.7					94	4.68	4.47	4.24	4.04	3.85
19.41	14.48	11.29	9.67	8.67	7.82	7.25	6.7					94	4.67	4.47	4.24	4.04	3.83
19.34	14.46	11.12	9.62	8.56	7.81	7.2	6.7					92	4.66	4.47	4.22	4.03	3.82
19.32	14	10.95	9.53	8.56	7.8	7.15	6.7					9	4.65	4.46	4.22	4.03	3.81
18.15	13.91	10.9	9.53	8.53	7.76	7.13	6.6					9	4.65	4.45	4.21	4.03	3.81
17.74	13.89	10.86	9.51	8.53	7.73	7.12	6.6					86	4.61	4.44	4.16	4.03	3.81
17.51	13.88	10.73	9.51	8.51	7.65	7.09	6.6					85	4.61	4.44	4.15	4.02	3.8
17.32	13.83	10.7	9.49	8.49	7.63	7.06	6.62	6.2	5.61	5.3	5.07	4.85	4.59	4.43	4.13	4.02	3.79
17.08	13.75	10.68	9.38	8.49	7.62	7.03	6.62	6.17	5.59	5.3	5.06	4.83	4.58	4.42	4.13	4.01	3.78
16.72	13.68	10.61	9.37	8.43	7.58	7.03	6.6	6.14	5.59	5.3	5.06	4.81	4.58	4.41	4.12	4	3.78
16.66	13.39	10.52	9.36	8.37	7.58	6.99	6.59	6.11	5.58	5.27	5.05	4.81	4.58	4.39	4.12	3.99	3.78
16.47	13.3	10.41	9.31	8.34	7.56	6.98	6.59	6.09	5.57	5.27	5.05	4.81	4.57	4.39	4.12	3.98	3.77

Fig. 10. Sample of data set for Coastal Point 700, corresponding to a tsunamigenic slope failure return period of 3350 yr. Runup is ranked in descending order in columns from left to right, with the magnitude of the 3350-yr and 500-yr tsunamis identified.

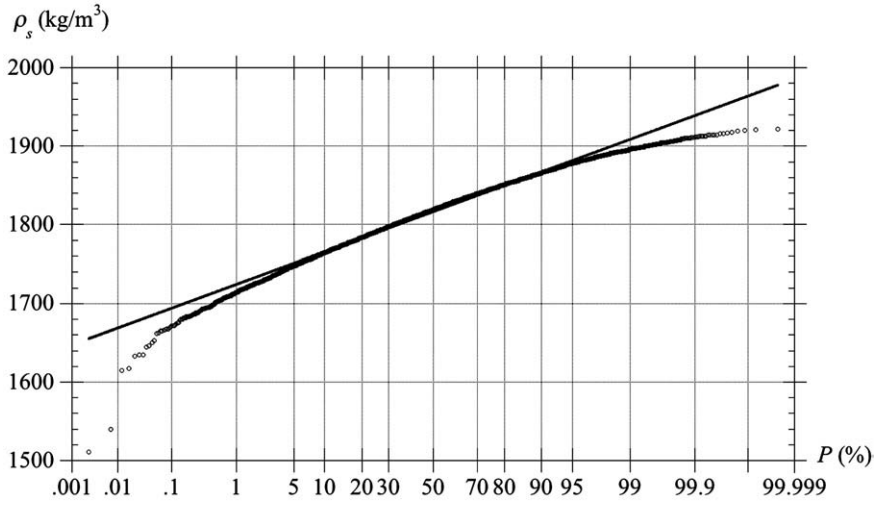

Fig. 11. MCS cumulative frequency distribution, compared to *normal* distribution fit ($R^2 = 0.989$), of the randomly generated slide density ρ_s (input parameter). With $m(\rho_s) = 1816.6$ kg/m^3 and $s(\rho_s) = 39.9$ kg/m^3.

bias statistical analyses and yield unrealistic results. To verify their relevance, these distributions were calculated based on model results, and compared to expected theoretical distributions or data when the latter was available. Such validations were performed up to very long return periods, such as 10,000 yr, using at least 10,000 simulations for each return period and transect.

Additionally, a multiple-part validation of the MCS slope stability analyses was performed, comprising: (i) a basic analysis of selected failure planes, with evaluations of safety factors at various stages of the slope stability methodology for translational failures; (ii) a comparison of MCS critical failure surfaces with those of the standard code SLOPE-W™ for rotational failures; (iii) a comparison of the coefficients of variation of soil properties used in the model with published data; and (iv) a comparison of failures predicted by the model to known submarine failure geometries (Booth et al., 1993). The latter validation ensures that only realistic failures are being considered in the eventual statistical analysis of tsunami runup.

The work by Booth et al. (1993) identified 179 individual landslides (i.e., SMFs) on the northeast U.S. Atlantic outer continental margin. The geometry and type of these SMFs varied widely, for instance: length varied between 0.3 and 380 km (the most frequent length being 2 to 4 km); width ranged from 0.2 to 50 km (the most frequent width being 1 to 2 km); and thickness widely varied from 10 to 650 m. The area of these SMFs ranged from 0.1 to 19,000 km^2, with two-third of all known slides in the region having an area of 10 km^2 or less. The majority of failures occurred for slopes of 4° or less, a few for slopes of 4–10°, and only very rarely for slopes between 10–12°. Booth et al. (1993) concluded that steep slopes (i.e., submarine canyon sidewalls, typically greater than 13°) are generally stable, with extremely rare slide occurrences. The types of failures ranged from block slides to debris flows, with the majority being debris slides (i.e., displaced mass of large coarse-grained sediment). The failure shape was found to be predominantly translational (57% of all cases) and occurring on an open slope morphological setting.

5.1. Distributions of input parameters

Figs. 11–13 show cumulative frequency distributions of SMF density, depth, and length, based on over 20,000 failures identified in the MCS model. Results clearly exhibit the expected *normal* or *log-normal* distributions for each parameter (R^2 close to 1 were obtained for each probability curve fit), and particularly within the typical 5–95% probability range. Additional verifications (not shown here) were done for slide thickness-to-length ratio (uniform distribution), width ratio (uniform

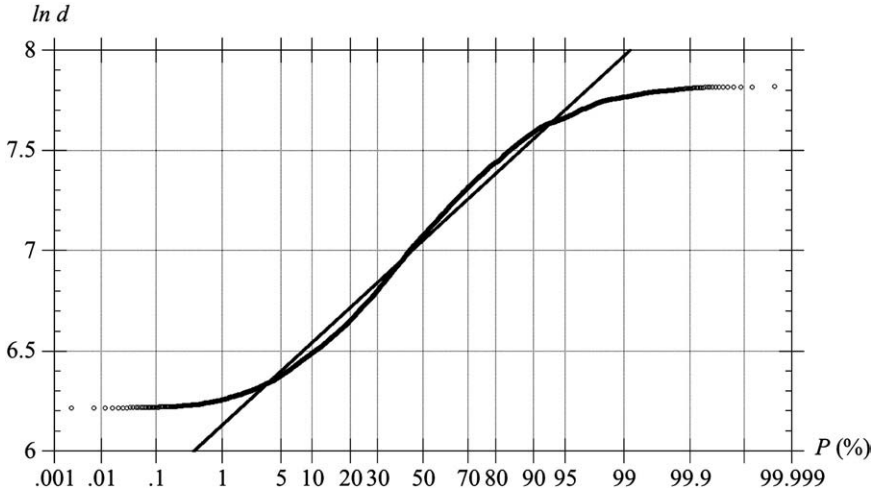

Fig. 12. MCS cumulative frequency distribution, as compared to *log-normal* distribution fit ($R^2 = 0.974$), of the randomly generated slide depth d (input parameter). With $m(d) = 1247$ m and $s(d) = 485$ m.

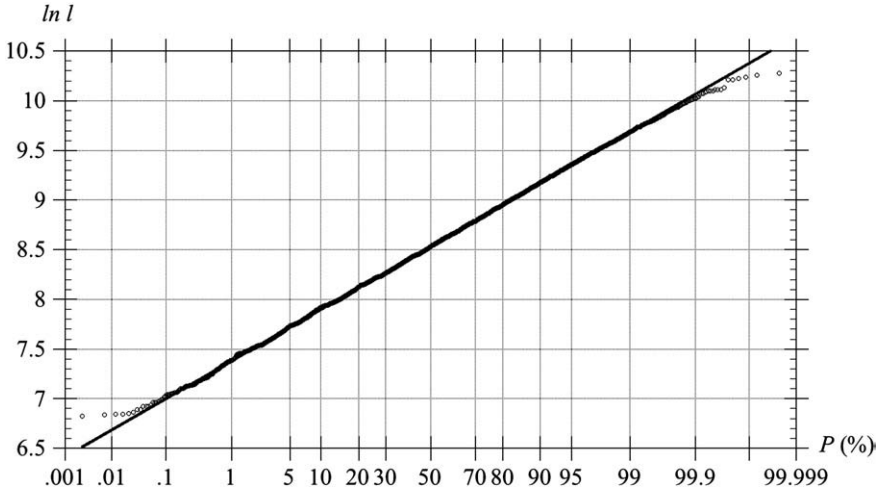

Fig. 13. MCS cumulative frequency distribution, as compared to *log-normal* distribution fit ($R^2 = 0.999$), for the randomly generated slide length l (input parameter). With $m(l) =$ 5749 m and $s(l) = 3024$ m.

distribution within the selected range), and tsunami direction of propagation with respect to the transect direction (normal distribution).

5.2. Slope stability

5.2.1. Translational failures

A three-stage method is used to compare the factor of safety FS_{MCS} computed in the MCS model using Eq. (7), to that obtained from the standard force equilibrium method for infinite slope failures (Duncan and Wright, 2005).

The first stage ensures that the selected failure plane is stable, with respect to the sediment strength properties, prior to specifying any triggering mechanism, by checking that the failure plane angle β selected by the model does not exceed the effective friction angle ϕ' of the sediment,

$$FS_1 = \frac{\tan\phi'}{\tan\beta}. \tag{32}$$

The second stage verifies that the inclusion of excess pore pressures, through R_u in Eq. (5), does not cause failure without seismic activity,

$$FS_2 = \left(1 - \frac{\Delta u}{g\rho_w(s-1)\cos\beta}\right)\tan\phi'. \tag{33}$$

The third stage considers seismic activity and: (i) checks the computation of FS_{MCS} within the model; and (ii) verifies that the slope

Table 3
Validation results for translational failures.

Transect no.	Angle β (°)	Friction angle ϕ' (°)	Density ρ_s (kg/m^3)	Sp. density s	Pore press. ratio R_u	$k = PHA/g$ (%)	FS_1 Eq. (32)	FS_2 Eq. (33)	FS_3 Eq. (12)	FS_4 Eq. (12)	FS_{MCS} MCS
19						0.0061	7.645	1.2	0.992	–	0.986
	4	28.13	1762.91	1.72	0.84	0.0056	–	–	–	1.006	1
16						0.0066	36.963	1.856	0.993	–	0.976
	1	32.83	1785.47	1.74	0.95	0.0062	–	–	–	1.022	1.005
44						0.0066	37.747	1.767	0.968	–	0.954
	1	33.38	1866.39	1.82	0.95	0.0059	–	–	–	1.017	1.004
29						0.0078	7.826	1.254	0.994	–	0.987
	4	28.69	1797.34	1.75	0.84	0.0073	–	–	–	1.007	1
3						0.0075	10.529	1.28	0.966	–	0.958
	3	28.89	1825.28	1.78	0.88	0.0063	–	–	–	1.007	1
8						0.008	11.119	1.345	0.989	–	0.979
	3	30.23	1773.18	1.73	0.88	0.0074	–	–	–	1.009	1
10						0.0089	18.68	1.605	0.993	–	0.979
	2	31.92	1792.01	1.74	0.91	0.0084	–	–	–	1.015	1.001
30						0.0088	4.427	1.173	0.998	–	0.993
	7	28.28	1784.76	1.74	0.74	0.0084	–	–	–	1.005	1
37						0.0089	6.216	1.23	0.989	–	0.982
	5	28.54	1780.33	1.73	0.8	0.0079	–	–	–	1.011	1.005
14						0.0099	12.406	1.492	1.002	–	0.989
	3	31.61	1729.98	1.68	0.88	0.0096	–	–	–	1.014	1.001
22						0.0086	10.743	1.385	0.996	–	0.986
	3	28.97	1784.47	1.74	0.87	0.008	–	–	–	1.016	1.007
33						0.009	19.22	1.599	0.974	–	0.992
	2	33.2	1729.1	1.79	0.92	0.0086	–	–	–	0.99	1.008
1						0.009	8.14	1.307	0.999	–	0.99
	4	29.65	1765.18	1.72	0.84	0.0087	–	–	–	1.008	1

Table 4
Validation results for rotational failures.

Input parameters: determined by Monte Carlo model							S_u / s'_v	FS_{MCS}	Safety factor				Case
l	d	T	β	ρ_s	R_u	$k = PHA/g$			FS (SLOPE-W™)				
(m)	(m)	(m)	(°)	(kN/m^3)		(%)			Bishop's	Ordinary	Janbu	Spencer	
1652.62	1245.53	133.22	7	18.09	0.39	0.0017	0.2041	**0.873**	**0.736**	0.736	0.723	0.736	Case 1
1220.29	1094.04	163.02	7	18.58	0.38	0.0017	0.2155	**0.965**	**0.985**	0.985	0.954	0.985	Case 2
3581.53	1792.24	287.9	3	18.88	0.68	0.009	0.1959	**0.998**	**0.986**	0.986	0.968	0.986	Case 3
1769.92	654.22	198.06	13	18.59	0.00	0.0065	0.2084	**0.998**	**0.942**	0.942	0.901	0.942	Case 4
2890.53	1617.33	182.11	4	18.36	0.48	0.0146	0.2054	**1.026**	**1.072**	1.072	1.058	1.072	Case 5
2108.52	1750.53	269.46	2	18.66	0.71	0.0146	0.1922	**1.044**	**1.181**	1.181	1.122	1.181	Case 6
1734.04	1482.49	189.64	4	18.237	0.37	0.0146	0.1964	**1.305**	**1.355**	1.355	1.289	1.355	Case 7

is failing for the minimum *PHA*. To do so, Eq. (7) is first solved for the same *PHA* (i.e., k) as determined by the model to cause failure [FS_3], and then for a *PHA* corresponding to a seismic return period of 10 yr less [FS_4]. The latter is to ensure that the *PHA* reported by the model is truly the minimum required to cause failure, and hence the return period of the event is accurate. The latter is vital for the accuracy of statistical analyses of the resulting tsunamis and the generation of hazard maps.

Table 3 shows validation results for 13 randomly selected translational failures. First, solely based on sediment properties, the safety factor [FS_1] is extremely large (ranging from 4 to 36), indicating very stable slopes especially at low failure angles (less than 5°; however, failures are known to have occurred within the region at such low angles). Second, the inclusion of excess pore pressures is not sufficient to cause failure without seismic activity [FS_2], even for the large magnitudes of R_u in these 13 failed cases. The magnitude range of FS_2 (1.20 to 1.86) indicates that these slopes, both naturally and in the model, remain stable at elevated pore pressures. Further, it is evident from the small magnitude of the *PHA*, which can realistically be found within this region (see values for the 13 cases), that seismic activity alone is not large enough to cause failure, without the inclusion of excess pore pressures. Third, once seismic activity is included into the validation analysis, together with excess pore pressure, the factor of safety [FS_3] decreases to below unity, confirming that both are required to cause failure. This safety factor compares well with the computed safety factor in the MCS model [FS_{MCS}]. Finally, the factor of safety corresponding to a seismic return period of 10 yr less [FS_4] is found greater than unity in all cases (but one: 0.99), confirming that failure would not occur at a lower seismic return period, and thus the minimum return period is truly being calculated within the Monte Carlo model.

5.2.2. Rotational failures

Rotational failures are validated by comparing MCS predictions to those of commercial software SLOPE-W™, in which effects of various triggering mechanisms can be modeled (e.g. pore pressures, seismicity, etc.), according to several methodologies (e.g., Bishop's Method, Ordinary Method of Slices, Janbu's Method, Spencer's Method, etc…). Because we can verify the overall safety factor found in the MCS model [FS_{MCS}], there is less need to validate the methods stage-by-stage, as was done above for translational failures.

While an agreement in the calculated safety factors (by both SLOPE-W™ and the MCS model) is required for validation, it is also critical to determine whether a reasonable agreement can be reached in the location of the failure surfaces. If the model assumes a deep failure, but the critical failure surface in SLOPE-W™ is shallow, then (even if the safety factors are similar) a bias may be introduced within the initial tsunami amplitude, thus altering the statistical analysis of the resulting runup. Alternately, if there is only a moderate correlation between safety factors, but there is a good correlation in the modes of failure, then it can be reasonably assumed that realistic failure surfaces are selected by the MCS model.

Conventional stability analyses, such as done by SLOPE-W™, locate a critical failure surface by evaluating many potential slip surfaces through a systematic search process, and identifying the surface with the minimum factor of safety. By contrast, in the MCS trials the model only selects a single failure surface at a time, and analyzes its stability. The randomly selected surface may not be the critical failure plane, as determined from conventional means. However, thousands of trial slip surfaces are evaluated along the same transect, with varying geometry, sediment properties, and ground accelerations, and it is expected that, upon convergence, this process will result in the identification of relevant critical failure planes.

Verifying that it is the case is the main purpose of this validation. Thus, Table 4 shows parameters and results for 7 randomly selected rotational failures in the simulations (CASE 1-7), with FS_{MCS} ranging from 0.837 to 1.305. The table shows that each of four methods used in SLOPE-W™ produces a factor of safety FS in good agreement with that determined by the MCS model. [To do so, we used the same starting point for the failure surface, sediment properties, and ground motions as used in MCS simulations, and set moderate constraints to the maximum length of the possible failure surfaces investigated by SLOPE-W™ ($\pm$25% of the length selected within the MCS model). The reason for the latter is to confine SLOPE-W™ to the same regional bathymetry that is being considered by the MCS model, so that a valid comparison of failure surfaces and safety factors can be made.] This is to be expected for an effective stress analysis on submerged slopes. The Janbu Method is only a force equilibrium analysis (the other methods satisfy moment equilibrium), but still produces a safety factor consistent with the other methods. The final step in the validation (not shown here) was to verify that the failures surfaces identified for those 7 cases in both the MCS model and in SLOPE-W™,

Table 5
Comparison of coefficient of variation to published values.

	Density		Bouyant density		Effective stress friction angle		Undrained strength ratio	
	MCS model	Published	MCS model	Published	MCS model	Published	MCS model	Published
Minimum	1492.31	–	468.31	–	28	–	0.190	–
Maximum	1954.90	–	930.90	–	39.96	–	0.240	–
Mean	1832.74	–	808.74	–	31.71	–	0.207	–
Std Deviation	41.90	–	41.90	–	1.48	–	0.010	–
CoV	2.3%	3-7%	5.2%	0–10%	4.7%	2–13%	5.1%	5–15%

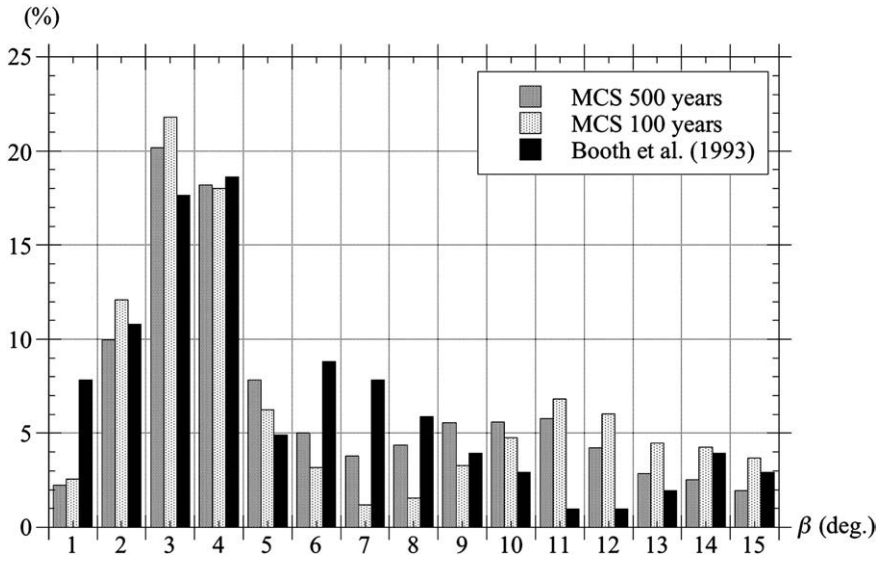

Fig. 14. Frequency of failure slope angle for MCS (100 and 500 yr PHA), as compared to observed failures (Booth et al., 1993). For the latter, the slope angles are determined at the site of the SMF origin.

using Bishop's Method as in the MCS model, were also in good agreement; this was found to be true in all cases.

5.3. Comparison of coefficient of variations for sediment properties

The final validation of slope stability analyses in the MCS model is to compare the ranges, as measured by the coefficients of variation [*CoV* = *s.d.* / *mean*], of distributions of sediment physical parameters found in the MCS model, to published values. A good agreement of these ranges will imply that the Monte Carlo model is not predicting trial sediment properties that could be considered *unrealistic* and bias the results. This validation is done in Table 5, for strength parameters and unit weights (bulk and buoyant), whose *CoVs* are found to be in good agreement with those published by Duncan and Wright (2005). [It should be noted that *CoV* values calculated from the MCS results are at the lower end of the ranges cited in the literature. In the case of the density parameter, the MCS value is slightly lower (difference of 0.7%) than the published range.]

5.4. Comparison of model results to known failures from geological evidence

The final validation of the MCS model outputs is to compare the distributions of failure parameters generated by the model with distributions known from geological evidence. The MCS model outputs tsunamigenic failures and their characteristics. Geological surveys, by Booth et al. (1993), provide evidence of SMFs over a span of approximately 200,000 yr [Chaytor et al. (2007) indicate that the majority of these slides are older than 10,000 yr]. It is not known, however, how many of these were tsunamigenic, but it is hoped nevertheless that distributions of their relevant parameters will be comparable with MCS predictions (i.e., for area, slope angle, and failure type).

For this comparison, the model was run with 50,000 trials for each transect, and information corresponding pertaining to the 100 and 500 yr *PHA* was collected. Distributions of failure slope angle, area, and type were compared. The agreement between observed and predicted types of failure (i.e., translational or rotational) and failure

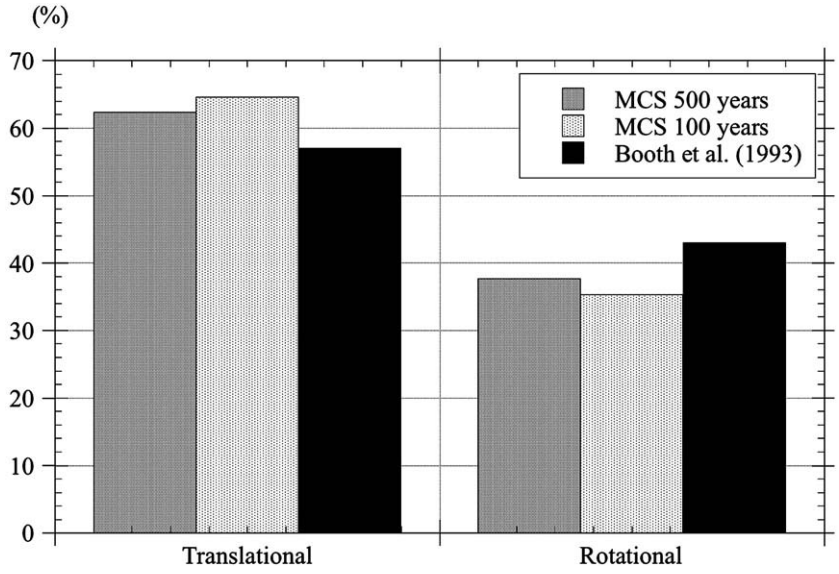

Fig. 15. Frequency of failure type for MCS (100 and 500 yr *PHA*), as compared to observed failures (Booth et al., 1993).

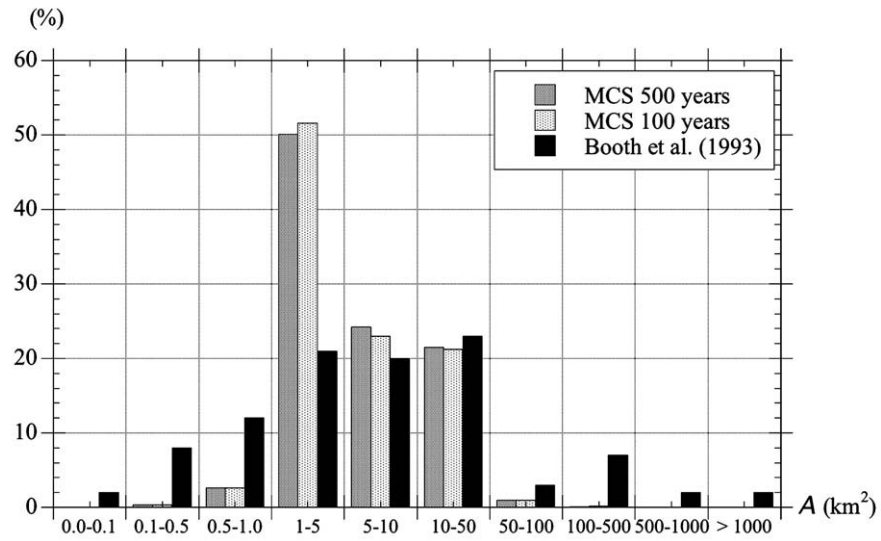

Fig. 16. Frequency of failure area for MCS (100 and 500 yr *PHA*), as compared to observed failures (Booth et al., 1993). Note, in the observations, slide area may be smaller than depicted, due to survey methodology used at the time.

slope angles appears reasonable in Figs. 14 and 15; the agreement is not as good for the failure area in Fig. 16. While it is noted by Booth et al. (1993) that the mean slide area may be smaller than observed, because of survey methodology used at the time of the study, the MCS model does not yield a slide with an area greater than 500 km^2 and only a negligible fraction of slides with an area greater than 100 km^2. Also, the MCS model predicts a larger percentage of medium size areas (1–5 km^2) and less small size areas than observed. Two main model parameters contribute to this discrepancy, sediment type and associated properties, and the determination of the lateral extents of the submarine landslide. Given the high degree of uncertainty regarding the sediment type data, due to the very small amount of available core data, it is reasonable to assume that, as more reliable geotechnical sediment data is obtained, the correlation of this distribution function with observations will improve. Overall, results, however, are deemed to yield a relatively good agreement between predicted and observed data for slope failures in the region, thus validating the outputs of the MCS model in this respect.

6. Results of the Monte Carlo model

6.1. Probability of tsunamigenic slope failure

When using the Monte Carlo model for complete analyses, 15,000 simulations were performed for each of the 45 transects (i.e., $N = 675{,}000$). Using the statistical analysis methodology described above, results yield a 15.5% probability of a tsunamigenic SMF, resulting from a 0.2% annual-probability (i.e., 500 yr) *PHA* event within the study area. As detailed before, the corresponding tsunamigenic SMF return period is 3350 yr (i.e., a 0.03% annual probability of occurrence).

The coastal runup associated with up to a 3350 yr tsunamigenic SMF was found to satisfy a log-normal probability distribution at each coastal point (e.g., Fig. 17 for Point 700). This is consistent with field observations or results of simulations of tsunami runup with a propagation model (e.g., Ioualalen et al., 2007). Based on these distributions, the 1% and 0.2%-annual-probability tsunami inundation

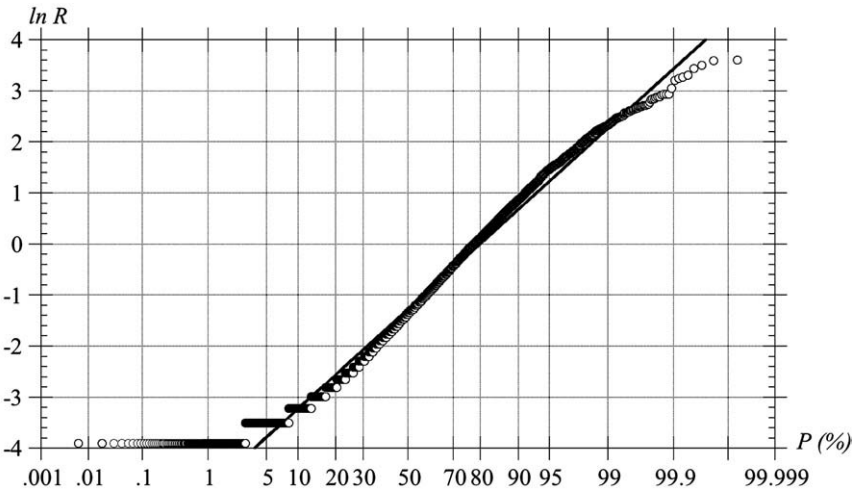

Fig. 17. MCS cumulative frequency distribution, compared to *log-normal* distribution fit ($R^2 = 0.978$), of the coastal runup calculated at Point 700.

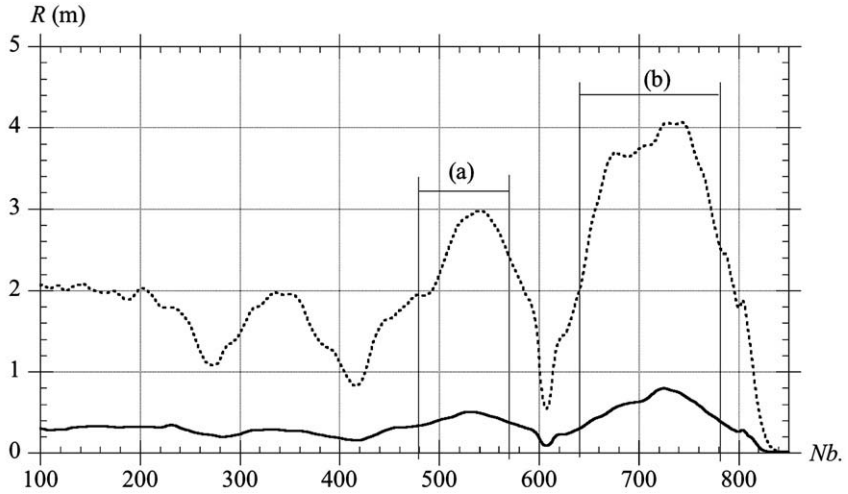

Fig. 18. MCS runup for design tsunamis of 1 (———) and 0.2 (- - - - -) % annual probability, as a function of coastal point number (Nb.), increasing from N to S. Coastal regions with relatively increased tsunami hazard are marked for points: (a) 480–570 (Long Island, NY) and (b) 640–780 (New Jersey coast).

levels (100, 500-yr design tsunamis) were calculated as discussed before, similar to standard methodologies adopted by FEMA and NOAA.

6.2. Upper U.S. East Coast tsunami hazard

Fig. 18 shows the SMF tsunami runup predicted along the studied section of U.S. coastline, for the 100 and 500 yr tsunami events; these range from 0.1 to 0.8 m and 0.5 to 4.2 m, in each case, respectively. No region of relatively elevated tsunami risk is identified in the 100 yr runups. However, for the 500 yr runups, two areas of elevated risk appear, with maximum runups reaching 3 m (a) and 4.2 m (b); these are the Hudson River estuary and Western Long Island coastline (NY) (a), and the New Jersey coastline (b). This first-order estimate of overall SMF tsunami hazard, in terms of 100 and 500 yr tsunami runup events, is thus found to be quite low at most locations, particularly as compared to the typical 100 yr hurricane storm surge in the region (approximately 5 m; USACE, 1988). However, two regions of relatively elevated hazard were identified; Fig. 19 shows coastal transects, in these, which yield the highest potential tsunamigenic landslide hazard, and marks the most affected coastal region (Cape May to Atlantic City, NJ).

Up to this point, maximum coastal runup (our measure of tsunami hazard) has been estimated by the initial tsunami depression above each SMF (i.e., using the "correspondence principle"). This assumption, however, neglects site-specific effects on tsunami propagation and transformation, which are governed by the local bathymetry and coastline topography. These effects can lead to significant wave refraction and shoaling, leading to tsunami focusing or de-focusing in some areas. While the absence of such effects in the model may still yield a relatively good first-order estimate of regional tsunami hazard (Figs. 18 and 19), the actual detailed coastal runup and inundation levels may vary greatly in some locations. It was deemed computationally prohibitive to perform full tsunami propagation simulations

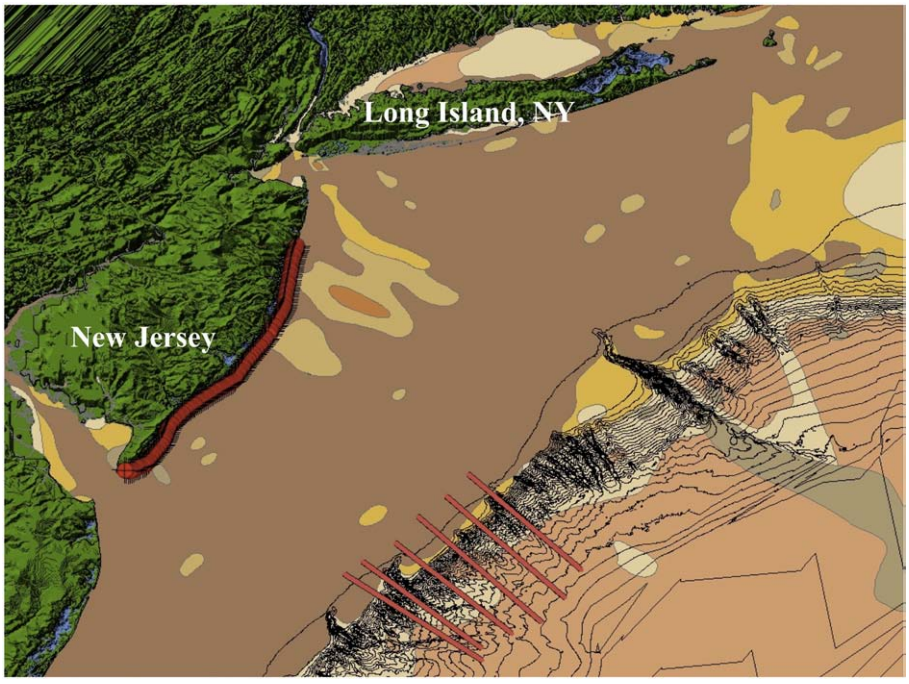

Fig. 19. Coastal transects yielding the highest potential tsunamigenic submarine landslide hazard (expressed in terms of runup), and the most affected coastal region (Cape May to Atlantic City, NJ; Fig. 18).

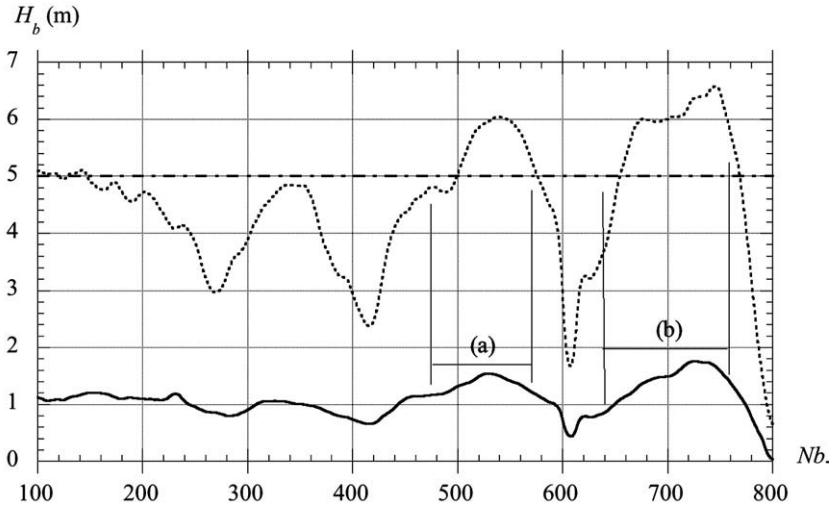

Fig. 20. Tsunami breaking height as a function of coastal points numbered increasingly from N to S (Nb.) (same line codes and (a), (b) definitions as in Fig. 18).

for each tsunamigenic SMF identified in the MCS model. Nevertheless, a simple estimate of breaking height was performed for each propagating tsunami, which included shoaling effects (as a function of a simplified nearshore bathymetry; Eqs. (24)–(27)), while preserving the same statistical methodology that produced runup results. Using this methodology, breaking wave heights were computed for the 100 yr and 500 yr events in Fig. 20, and corresponding breaking distances from shore in Fig. 21. As could be expected, breaking wave heights are found to follow the same trend as runup, with the same two regions (a) and (b) of relatively elevated risk. Breaking heights, however, are larger than predicted runup and, particularly, the 500 yr tsunami breaking height (at an average 265 m offshore), is greater than the 5 m hurricane storm surge, in most of regions (a) and (b) of Fig. 20.

In Fig. 21, the distance from the shoreline to each estimated tsunami breaking point (Eq. (26)) shows that, in the two regions of elevated risk: (a) the 500 yr tsunami breaking distance is 280 m in average (76 m for the 100 yr tsunami); (b) the average 500 yr tsunami breaking distance is 251 m (61 m for the 100 yr tsunami). This estimated location of tsunami breaking can be used to either increase or decrease the potential hazard along localized coastal points. As waves break, their energy is dissipated and both their height and velocity decrease. Therefore, as the breaking distance from shore increases, there is a wider surf zone to cause more energy dissipation before waves reach the shore. However, an increased distance may also correspond to larger incoming tsunamis, with larger breaking wave heights (as can be seen by looking at Fig. 20).

Finally, computations of tsunami travel times yield $t_0 = 126$–164 min, with a mean $\bar{t}_0 = 134$ min, for the 100 yr event, and $t_0 = 125$–161 min, with $\bar{t}_0 = 135$ min, for the 500 yr event. Hence, assuming the SMF (or the generated tsunami) can be detected at the source, there should be ample warning time, of at least 2 h in the region.

7. Conclusions

Locat and Lee (2002) identified 9 major challenges in the study of SMFs: (i) the need to improve sediment sampling techniques in conjunction with in-situ testing; (ii) the integration of 3D seismic modeling into slope stability analysis; (iii) the use of long core sampling to determine the frequency of catastrophic failures; (iv) the identification and understanding of the physical process of the sediment transition from pre-failure to post-failure conditions, to better predict the initial acceleration and the transition of the failed mass to a fluid-like debris flow; (v) hazard assessment; (vi) monitoring the movement and mobilization of actual slide events; (vii) determining and incorporating the role of subsurface water flow and gas hydrate

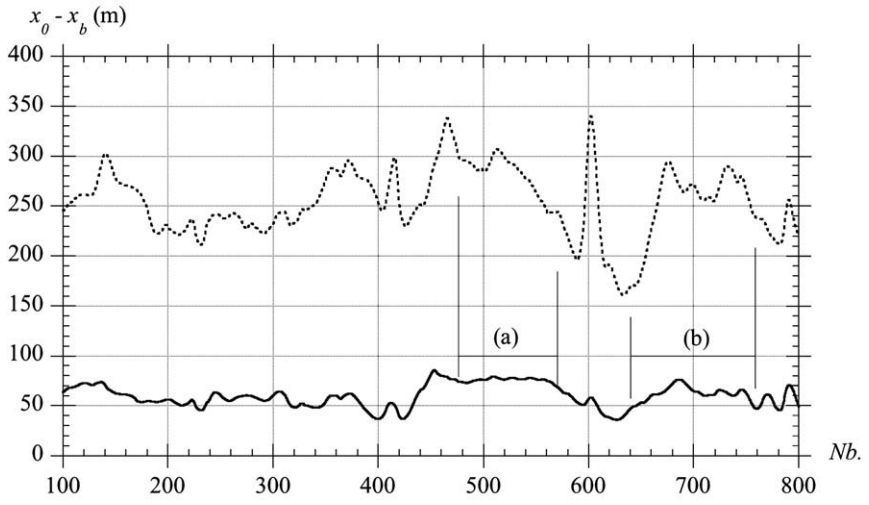

Fig. 21. Average tsunami breaking distance from shore as a function of coastal points numbered increasingly from N to S (Nb.) (same line codes and (a), (b) definitions as in Fig. 18).

dissociation in slope stability modeling; (viii) evaluating the mechanics of giant slide events and improving the current understanding of their great run-out distances; and (ix) development of standard criteria to classify seafloor deposits as either landslides or migrating sediment waves.

This work addresses the hazard assessment (item (v)) of submarine failures (SMF), following a probabilistic approach. While a SMF, by itself, poses a significant risk to infrastructure (e.g., cables, pipelines, foundations of offshore structures, etc…), there is minimal direct risk to human life. However, the indirect risk to human life increases substantially when considering the possibility of a resulting tsunami. Therefore, here, the hazard presented by the SMF is not measured in terms of physical characteristics (e.g., size and kinematic velocity), but in its tsunami potential, defined by runup (or coastal inundation levels).

A Monte Carlo Simulation (MCS) model was developed, refined, and validated to estimate hazard along the upper U.S. East Coast, from seismically triggered tsunamigenic SMF, expressed in terms of design tsunami runup (and breaking wave height) levels, at a given annual probability of exceedance. The model framework incorporates actual bathymetry for the continental shelf, and the seismic data was characterized using a U.S. Geological Survey database (USGS, 2007). To estimate the peak horizontal ground (bedrock) acceleration [*PHA*], for more efficiency, the study area was discretized into a 0.1° grid and all cells representing a location on land removed; in each cell, the natural logarithm of the *PHA* was curve fitted to the probability of exceedance from the database, and these equations were then used to generate *PHA* for any given seismic return period. Considering the lack (or paucity) of detailed information about sediment types and stratigraphy, depth to bedrock, and sediment properties, necessary for a site-specific response analysis, the pseudo-static seismic coefficient was assumed equal to the *PHA*.

Due to the limited geotechnical investigations and data available, surficial sediment profiles from the Continental Margin Mapping (CONMAP) database were used to classify the sediment types within the region. Each identified sediment type was assigned distributions within a set range of physical and strength properties. Furthermore, the sediment along each transect is not homogeneous laterally; however, due to the limited geotechnical investigations it was assumed that the sediment is vertically homogenous. Furthermore, the unknown depth to bedrock within the region was assumed to be greater than the maximum failure thickness.

Based on the single coring data available for the region (ODP Leg 174A), a potential for high levels of initial (excess) pore pressures was noted. To account for these and additional pore pressures that could be generated during seismic activity, an empirical reduction in shear strength of the sediment, as a function of pore pressures (above hydrostatic conditions), was incorporated into the effective stress, in slope stability analyses performed within the MCS model.

Once a trial slip surface is chosen in the MCS model, the *PHA* curve for that location is used to determine values of *PHA* for different annual rates of exceedence. Increasing values of *PHA* are applied until the slip surface fails (or the *PHA* return period exceeds 750 yr). Depending on the sediment type, an appropriate limit equilibrium equation is utilized to determine stability (i.e., Infinite Slope for cohesionless sediment; Modified Bishop's Method for cohesive sediments). All the failures are then cataloged according to a desired seismic triggering event (e.g., 100 or 500 yr ground motion).

Once a failure is deemed to occur, the model determines the magnitude (if any) of the resulting tsunami and coastal runup. A filter of 0.02 m was applied to define the minimum initial tsunami amplitude to be considered tsunamigenic. The tsunami wave then propagated onshore and corresponding runup, travel time, breaking height, etc…, were computed for each coastal point.

After all simulations were completed, a relevant statistical methodology was established and validated, to calculate the probability of a seismically triggered tsunamigenic failure and the corresponding potential (coastal) hazard (in terms of an annual probability of exceedance for tsunami runup). This methodology is derived from current methods used to assess the potential hazard from floods, hurricanes, and earthquakes, and yields similar hazard maps. In this new methodology (i.e., as compared to earlier versions of this work by Maretzki et al., 2007), the annual probability of tsunamigenic failure is determined as the joint probability of the probability of failure (determined by the MCS model) and the annual probability of the seismic trigger. Therefore, the runup data resulting from random MCS trials, is expected to contain on average a tsunami runup corresponding to this event, from which the 100 and 500 yr tsunami events can be obtained. In this work the overall return period for tsunamigenic SMFs in the region was found to be approximately 3350 yr.

Validation of the model is paramount to ensuring the accuracy of the estimated tsunami hazard. Therefore, a thorough validation process was developed and implemented, for each phase of model development, based on comparisons to known geological evidence of failures, known parameter distributions, published coefficients of variation, and standard engineering slope stability practices (including using commercial software). The model was thus found to agree reasonably well with all validation data.

For 100 and 500 yr design tsunamis, the model predicts relatively small tsunami runup along the U.S. East coast. The 100 yr tsunami event has a peak runup of less than 1 m in the region, and identifies only one region (the New Jersey Coast) of slightly elevated hazard. The 500 yr tsunami event, however, clearly points at two regions of elevated hazard, Long Island, NY (with a peak runup of approximately 3 m) and the New Jersey Coast (with a peak runup of approximately 4 m).

To a first-order estimate, these runup levels appear sufficiently below those of a 100 yr hurricane surge of about 5 m (USACE, 1988), to be discarded as the main flooding hazard in the region (Fig. 18). However, it must be emphasized that this is only a first-order estimate, for the main purpose of identifying regions of elevated tsunami hazards on a regional scale. Local effects (e.g., fine-grid bathymetry, non-simplified shorelines, wave refraction and shoaling, etc…) could potentially create significant increases in runup (and resulting inundation). Hence, particularly for a 500 yr event, tsunami inundation could locally potentially be greater than the typical 100 yr storm surge (5 m) along this Atlantic margin. This is especially true off of Atlantic City, NJ (Fig. 19), as illustrated in Fig. 20, with a peak breaking height of 6 to 7-m. Further, the wave breaking distance from the shoreline was found to be relatively small (approximately 265 m for the 500 yr event; Fig. 21) indicating that the energy dissipation and reduction in wave height and celerity before impacting the shore are relatively low, thus increasing the potential inundation hazard. Finally, calculated tsunami travel time estimates show that, assuming the SMF (or the generated tsunami) could be detected at the source, there should be ample warning time of at least 2 h in the region.

In closing, the combination of nearshore breaking and elevated wave height at breaking appears to offer a richer estimate of tsunami hazard, in this analysis, than solely based on a simple estimate of runup, derived from initial tsunami amplitude, which may significantly underestimate the true magnitude of such hazard. Fig. 19 marks transects found most susceptible to SMF in MCS simulations, as well as the most likely severely impacted coastal area off of NJ. In future work, this region of the continental shelf should be the focus of more detailed geotechnical investigations, and actual tsunami generation and propagation modeling. Finally, first-order estimates of flooded areas could be inferred based on static heights, from runup distributions predicted along the coast, such as in Fig. 18. However, local flooding should be best determined from more accurate direct regional tsunami and local flooding simulations, particularly in the identified regions of elevated hazard; this could also be the object of future work.

Notations

The following symbols are used in this paper:

β	seafloor slope angle;
c'	effective sediment cohesion;
c_g	long wave group velocity;
CoV	coefficient of variation;
d	depth below sea level;
$\bar{E}$	time-averaged wave energy;
ε	empirical coefficient;
ϕ'	effective friction angle;
FS	factor of safety;
$\Delta\Phi$	maximum angular displacement;
g	gravitational acceleration;
H	local wave height;
H_b	wave height at breaking;
H_o	initial wave height;
h	local water depth;
h_b	water depth at breaking;
h_o	initial water depth;
η_{oR}	initial tsunami amplitude, rotational failures;
η_{oT}	initial tsunami amplitude, translational failures;
κ	breaking index;
k	pseudo-static seismic coefficient;
l	SMF length;
λ_{oR}	characteristic tsunami wavelength, rotational failures;
λ_{oT}	characteristic tsunami wavelength, translational failures;
P_f	probability of slope failure;
P_{max}	maximum annual probability;
P_{SMF}	annual probability of tsunamigenic slope failure;
P_{PHA}	annual probability of a given seismic ground motion;
PHA	peak horizontal ground (bedrock) motion;
R	runup;
R_{ur}	stress reduction factor, rotational failures;
R_{ut}	stress reduction factor, translational failures;
r	radius of rotational failure;
ρ_s	sediment density;
ρ_w	water density;
$\Re$	randomly generated number;
S	shear force;
S_u	undrained shear strength;
S_u/σ'_{vo}	undrained shear strength ratio;
S_{oR}	characteristic distance of motion, rotational failures;
S_{oT}	characteristic distance of motion, translational failures;
s	sediment specific density;
σ'	normal effective stress on the failure plane;
σ'_v	vertical effective stress;
T	SMF thickness;
t_o	tsunami arrival time;
$\bar{t}_0$	average tsunami arrival time;
τ_d	shear stress on the failure plane;
Δu	change in pore pressure;
V	SMF volume;
W	total SMF weight;
W'	buoyant SMF weight;
w_r	SMF width, rotational failure;
w_t	SMF width, translational failure; and
Δx	change in distance from SMF origin to location of wave breaking.

Acknowledgments

The authors acknowledge partial financial support from URI Ocean Engng., for the work performed here. URI-OCE does not necessarily endorse the methodologies followed and conclusions expressed in this paper, which are solely the authors' opinions. Furthermore, the authors wish to thank anonymous reviewers and the editor for their constructive and insightful reviews of their work, which they believe helped greatly improve the manuscript.

References

Booth, J.S., Circe, R.C., Dahl, A.G., 1985. Geotechnical characterization and mass-movement potential of the United States North Atlantic Continental Slope and Rise. Tech. Rep. U.S. Geological Survey, pp. 85–123.

Booth, J.S., O'Leary, D.W., Popenoe, P., Danforth, W.W., 1993. U.S. Atlantic Continental Slope Landslides: their distribution, general attributes, and implications. In: Schwab, W.C., Lee, H.J., Twichell, D.C. (Eds.), Submarine Landslides: Selected studies in the U.S. Exclusive Economic Zone. U.S. Geological Survey Bulletin 2002, pp. 14–22.

Canals, M., Lastras, G., Urgeles, R., Casamor, J.L., Mienert, J., Cattaneo, A., De Batist, M., Haflidason, H., Imbo, Y., Laberg, J.S., Locat, J., Long, D., Longva, O., Masson, D.G., Sultan, N., Bryn, P., 2004. Slope failure dynamics and impacts from seafloor and shallow sub-seafloor geophysical data: case studies from the COSTA project. Mar. Geol. 213, 9–72.

Chaytor, J.D., Twitchell, D.C., Ten Brink, U.S., Buczkowski, B.J., Andrews, B.D., 2007. Revisiting submarine mass movements along the U.S. Atlantic Continental Margin: implications for tsunami hazards. Submarine Mass Movements and their Consequences, 3rd Intl. Symp. Springer, pp. 395–404.

Chaytor, J.D., ten Brink, U.S., Solow, A.R., Andrews, B.D., 2009. Size Distribution of Submarine Landslides along the U.S. Atlantic Margin. Mar. Geol. 264, 16–27 (this issue).

Day, S.J., Watts, P., Grilli, S.T., Kirby, J.T., 2005. Mechanical models of the 1975 Kalapana, Hawaii earthquake and tsunami. Marine Geology 215 (1–2), 59–92.

Dean, R.G., Dalrymple, R.A., 1984. Water Wave Mechanics for Engineers and Scientists. Prentice Hall.

Di Risio, M., Bellotti, G., Panizzo, A., De-Giroamo, P., 2008. Three-dimensional experiments on landslide generated waves at a sloping coast. *Coastal Engng.* (submitted).

Duncan, M.J., Wright, S.G., 2005. Soil Strength and Slope Stability. John Wiley & Sons, Inc., Hoboken, NJ.

Enet, F., 2006. *Tsunami generation by underwater landslides*. Ph.D Dissertation, Department of Ocean Engineering, University of Rhode Island.

Enet, F., Grilli, S.T., 2005. Tsunami landslide generation: modelling and experiments. Proc. 5th Intl. on Ocean Wave Measurement and Analysis (WAVES 2005, Madrid, Spain, July 2005). IAHR Publication. paper 88, 10 pps.

Enet, F., Grilli, S.T., 2007. Experimental study of tsunami generation by three-dimensional rigid underwater landslides. J. Waterw. Port Coast. Ocean Eng. 133 (6), 442–454.

Enet, F., Grilli, S.T., Watts, P., 2003. Laboratory experiments for tsunamis generated by underwater landslides: comparison with numerical modeling. Proc. 13th Offshore and Polar Engng. Conf. (ISOPE03, Honolulu, USA, May 2003), pp. 372–379.

Elsworth, D., Day, S.J., 1999. Flank collapse triggered by intrusion: the Canarian and Cape Verde Archipelagoes. J. Volcanol. Geotherm. Res. 94, 323–340.

Fine, I.V., Rabinovich, A.B., Bornhold, B.D., Thomson, R., Kulikov, E.A., 2005. The Grand Banks landslide-generated tsunami of November 18, 1929: preliminary analysis and numerical modeling. Mar. Geol. 215, 45–57.

Goodbred, S.L., Krentz, S., LoCicero, P.V., 2006. Evidence for a newly discovered 2300-year-old tsunami deposit from Long Island, New York. Eos, Trans. — Am. Geophys. Union 87 (52) Fall Meet. Suppl., Abstract OS43C-0681.

Grilli, S.T., Watts, P., 1999. Modeling of waves generated by a moving submerged body. Applications to underwater landslides. Eng. Anal. Bound. Elem. 23, 645–656.

Grilli, S.T., Watts, Ph., 2001. Modeling of tsunami generation by an underwater landslide in a 3D-NWT. Proc. 11th Offshore and Polar Engng. Conf. (ISOPE01, Stavanger, Norway, June 2001), vol. III, pp. 132–139.

Grilli, S.T., Watts, P., 2005. Tsunami generation by submarine mass failure. I: modeling, experimental validation, and sensitivity analyses. J. Waterw. Port Coast. Ocean Eng. 131 (6), 283–297.

Grilli, S.T., Vogelmann, S., Watts, P., 2002. Development of a 3D Numerical Wave Tank for modeling tsunami generation by underwater landslides. Eng. Anal. Bound. Elem. 26 (4), 301–313.

Grilli, S.T., Ioualalen, M., Asavanant, J., Shi, F., Kirby, J., Watts, P., 2007. Source constraints and model simulation of the December 26, 2004 Indian Ocean Tsunami. J. Waterw. Port Coast. Ocean Eng. 33 (6), 414–428.

Harr, M.E., 1987. Reliability Based Design in Civil Engineering. Dover Publications Inc., Mineola, New York.

Haugen, K.B., Lovholt, F., Harbitz, K.B., 2005. Fundamental mechanisms for tsunami generation by submarine mass flows in idealized geometries. Mar. Pet. Geol. 22, 209–217.

Heinrich, P., 1992. Nonlinear water waves generated by submarine and aerial landslides. J. Waterw. Port Coast. Ocean Eng. 118 (3), 249–266.

Hildenbrand, A., Gillot, P.Y., Soler, V., Lahitte, P., 2003. Evidence for a persistent uplifting of La Palma (Canary Island), inferred from morphological and radiometric data. Earth Planet. Sci. Lett. 210, 277–289.

Ioualalen, M., Asavanant, J., Kaewbanjak, N., Grilli, S.T., Kirby, J.T., Watts, P., 2007. Modeling the 26th December 2004 Indian Ocean tsunami: case study of impact in Thailand. J. Geophys. Res. 112, C07024.

Knight, W., 2006. Modeling predictions of the Gulf and southern Atlantic coast tsunami impacts from a distribution of sources. Sci. Tsunami Hazard 24, 304–312.

Ladd, C.C., Foote, R., 1974. New design procedure for stability of soft clays. J. Geotech. Eng. Div. 100 (7), 763–786.

Liu, P.L.-F., Wu, T.-R., Raichlen, F., Synolakis, C.E., Borrero, J.C., 2005. Runup and rundown generated by three-dimensional sliding masses. J. Fluid Mech. 536, 107–144.
Locat, J., Lee, H., 2002. Submarine landslides: advances and challenges. Can. Geotech. J. 39, 193–212.
Locat, J., Desgagnes, P., Leroueil, S., Lee, H.J., 2003. Stability analysis of the Hudson Apron slope, off New Jersey, USA. In: Locat, J., Mienert, J. (Eds.), Submarine Mass Movements and Their Consequences. Kluwer Academic Publishers, pp. 267–280.
Locat, J., Lee, H.J., Locat, P., Irman, J., 2004. Numerical analysis of the mobility of the Palos Verdes debris avalanche, California, and its implication for the generation of tsunamis. Mar. Geol. 203, 269–280.
Lynett, P., Liu, P.L.-F., 2003. A numerical study of submarine–landslide-generated waves and runup. Proc. R. Soc. Lond., Coast, Oc. Eng., A 458, 2,885–2,910.
National Oceanic and Atmospheric Administration (NOAA), 2008. National Geophysical Data Center — Historical Tsunami Database. http://www.ngdc.noaa.gov/hazard/tsu_db.shtml.
Nowak, A.S., Collins, K.R., 2000. Reliability of Structures. McGraw-Hill International Editions, Civil Engineering Series, McGraw-Hill Companies, Inc.
Maretzki, S., 2006. Numerical Simulation of Tsunami Hazard Maps for the U.S. East Coast. *Masters Thesis*. Department of Ocean Engineering, University of Rhode Island, 187 pp.
Maretzki, S., Grilli, S.T., Baxter, C.D.P., 2007. Probabilistic SMF tsunami hazard assessment for the upper East Coast of the United States. In: Lykousis, V., Sakellariou, D., Locat, J. (Eds.), Proc. 3rd Intl. Symp. on Submarine Mass Movements and their Consequences (Santorini, Greece, October 2007). Springer, pp. 377–386.
Ocean Drilling Program (ODP), Leg 174A, Continuing the New Jersey Mid-Atlantic Sea-Level Transect. http://www-odp.tamu.edu/publications/leg_ndx/174andex.htm. (2008).
Pérignon, Y., 2006. *Tsunami Hazard Modeling.* Senior Engineering Thesis. Department of Ocean Engineering, University of Rhode Island and Ecole Centrale de Nantes, 40 pps.
Piper, D.J.W., Cochnot, P., Morrison, M.L., 1999. The sequence of events around the epicenter of the 1929 Grand Banks earthquake: initiation of debris flows and turnidity current inferred from sidescan sonar. Sedimentology 46, 79–97.
Piper, D.J.W., Mosher, D.C., Gauley, B.-J., Jenner, K., Campbell, D.C., 2003. The chronology and recurrence of submarine mass movements on the continental slope off Southeastern Canada. In: Locat, J., Mienert, J. (Eds.), Submarine Mass Movements and their Consequences. Klüwer Academic Publishers, pp. 299–306.
Poppe, L.J., Williams, S.J., Paskevich, V.F., 2005. U.S. geological survey East-Coast sediment analysis: procedures, database, and GIS data. Tech. Rep. 2005–1001. U.S. Geological Survey.
Rabinovich, A.B., Thomson, R.E., Bornhold, B.D., Fine, I.V., 2003. Numerical modeling of tsunamis generated by hypothetical landslides in the Strait of Georgia, British Columbia. Pure Appl. Geophys. 160, 1273–1313.
Seed, H.B., 1979. onsiderations in the earthquake-resistant design of earth rockfill dams. Geotechnique 29 (3), 215–263.
Tappin, D.R., Watts, P., McMurtry, G.M., Lafoy, Y., Matsumoto, T., 2001. The Sissano, Papua New Guinea tsunami of July 1998 — offshore evidence on the source mechanism. Mar. Geol. 175, 1–23.
Tappin, D.R., Watts, P., McMurtry, G.M., Lafoy, Y., Matsumoto, T., 2002. Prediction of slump generated tsunamis: the July 17th 1998 Papua New Guinea event. Sci. Tsunami Hazards 20 (4), 222–238.
Tappin, D.R., Watts, P., Grilli, S.T., 2008. The Papua New Guinea tsunami of 1998: anatomy of a catastrophic event. Nat. Hazards Earth Syst. Sci. 8, 243–266. www.nat-hazards-earth-syst-sci.net/8/243/2008/.
Terzaghi, K., 1950. Mechanics of landslides. (Berkeley Vol.). Proc. Geotech. Soc. Of America, Boulder, CO, November, pp. 83–123.
Tinti, S., Bortolucci, E., Chiavettieri, C., 2001. Tsunami excitation by submarine slides in shallow water approximation. Pure Appl. Geophys. 158, 759–797.
Titov, V.V., Rabinovich, A.B., Mofjeld, H.O., Thomson, R.E., Gonzalez, F.I., 2005. The global reach of the 26 December 2004 Sumatra tsunami. Science 309, 2045–2048.
Trifunac, M.D., Hayir, A., Todorovska, M.I., 2002. Was Grand Banks event of 1929 a slump spreading in two directions ? Soil Dyn. Earthqu. Eng. 22, 349–360.
United States Army Corp of Engineers [USACE], 1988. Tidal Flood Profiles; New England Coastline. Hydraulics and Water Quality Section, New England Division, United States Army Corps of Engineers.
United States Geological Survey (USGS), 2007. USGS National Seismic Hazard Maps. http://earthquake.usgs.gov/research/hazmaps.
Ward, S.N., 2001. Landslide tsunami. J. Geophysical Res., 106(11), 201–211, 215.
Ward, S.N., Day, S., 2001. Cumbre Vieja Volcano—potential collapse and tsunami at La Palma, Canary Islands. Geophys. Res. Lett. 28, 397–400.
Watts, P., 2004. Probabilistic predictions of landslide tsunamis off Southern California. Mar. Geol. 203, 281–301.
Watts, P., Grilli, S.T., 2003. Tsunami generation by deformable underwater landslides. Proc. 13th Offshore and Polar Engng. Conf. (ISOPE03, Honolulu, USA, May 2003), pp. 364–371.
Watts, P., Imamura, F., Grilli, S.T., 2000. Comparing model simulations of three benchmark tsunami generation cases. J. Sci. Tsunami Hazard 18 (2), 107–123.
Watts, P., Grilli, S.T., Kirby, J.T., Fryer, G.J., Tappin, D.R., 2003. Landslide tsunami case studies using a Boussinesq model and a fully nonlinear tsunami generation model. Nat. Hazards Earth Syst. Sci. 3, 391–402.
Watts, P., Grilli, S.T., Tappin, D.R., Fryer, G.J., 2005a. Tsunami generation by submarine mass failure. II: predictive equations and case studies. J. Waterw. Port Coast. Ocean Eng. 131 (6), 298–310.
Watts, P., Ioulalen, M., Grilli, S.T., Shi, F., Kirby, J.T., 2005b. Numerical simulation of the December 26, 2004 Indian Ocean Tsunami using a higher-order Boussinesq model. Proc. 5th Intl. on Ocean Wave Measurement and Analysis (WAVES 2005, Madrid, Spain, July 2005). IAHR Publication. paper 221, 10 pps.